Frontier Research Institute for Interdisciplinary Sciences
Tohoku University

Event Horizon Telescope

Theoretical Astrophysics
Tohoku University

ブラックホールジェット研究の新展開

當真 賢二 (TOMA Kenji)
東北大学 学際科学フロンティア研究所 / 理学研究科

第49回 天文・天体物理若手夏の学校@ロワジールホテル豊橋 2019/7/30-8/2

2019年度 第49回

~~若手~~・天体物理若手夏の学校

天文？

日程：2019年7月30日(火)〜8月2日(金)

会場：ロワジールホテル豊橋

主催：天文・天体物理若手の会

目次

Outline

1. ジェットの観測的性質
2. ジェットの物理の諸問題
    - 回転BH駆動
    - MHD加速
3. Event Horizon Telescope (EHT)
4. EHT観測でジェット駆動理論を確定できるか

5. 偏光とダークマターと惑星形成の学際研究

ブラックホールジェット (BH jets)

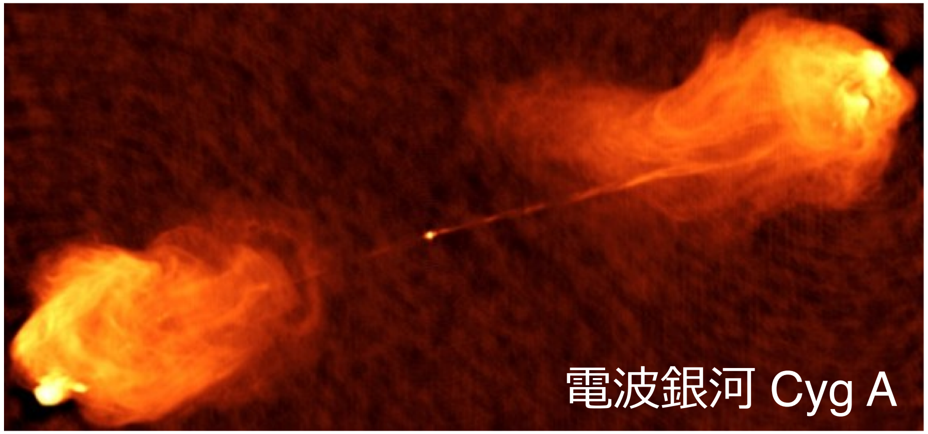

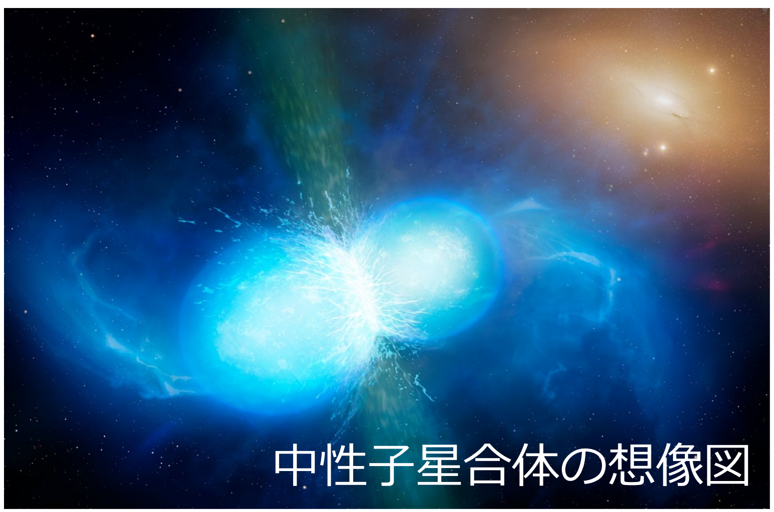

- 他にX線連星や潮汐破壊現象など
- 莫大なエネルギー放出！
- 相対論とプラズマ物理に関わる問題
- 広い分野に関連
  - 銀河進化への影響
  - 初代星ガンマ線バースト？
  - 重力波・ニュートリノ・宇宙線
- 観測の進展が著しい

活動銀河核ジェット (AGN jets)

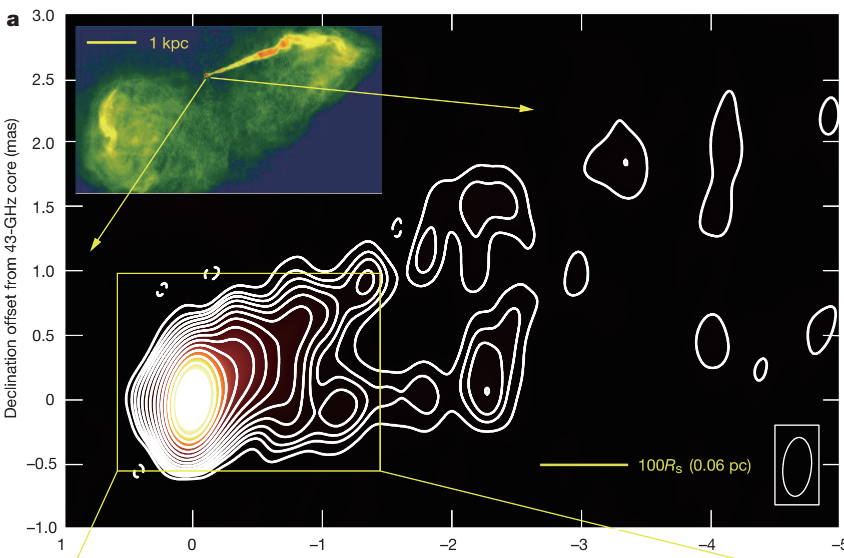

Hada+2011

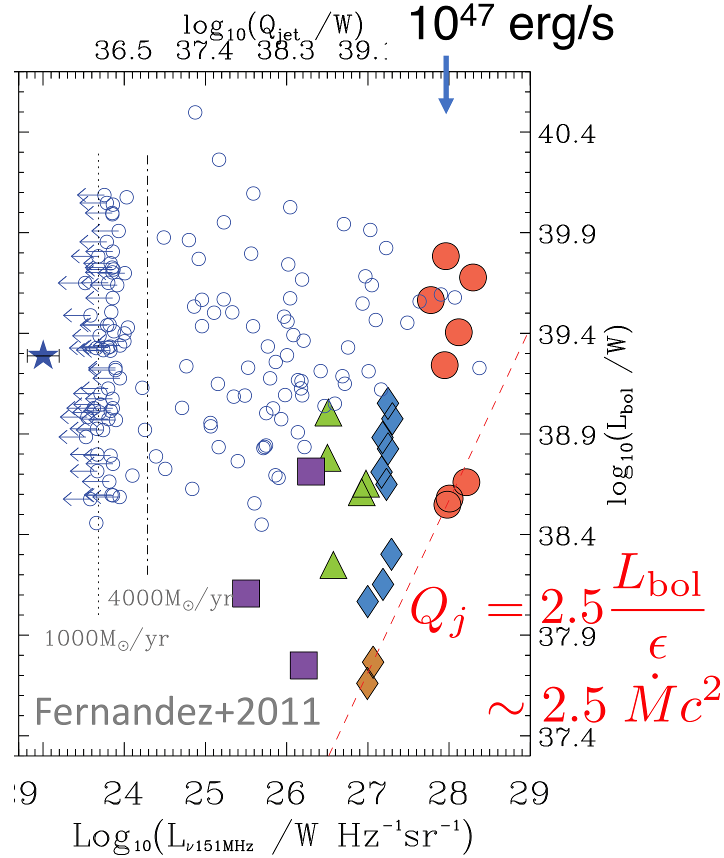

Fernandez+2011

静止

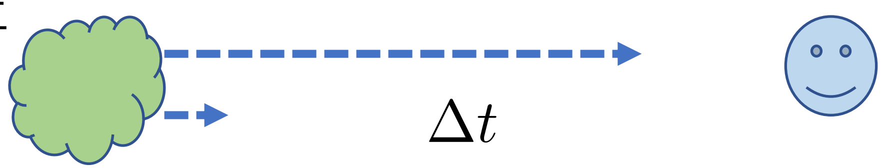

観測者に向かって v で運動

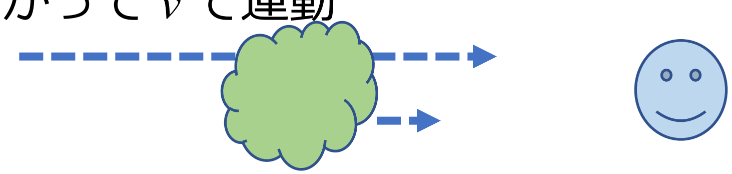

$$\Delta\tilde{t} = \Delta t(1 - v/c)$$

- 典型的に~100 kpcサイズ
- シンクロトロン放射
- 超光速運動 -> γ ~ 5-50?

ガンマ線バースト (GRBs)

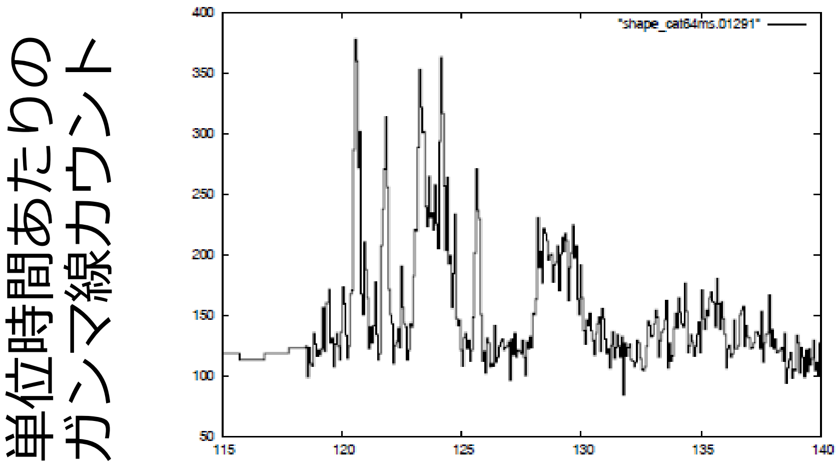

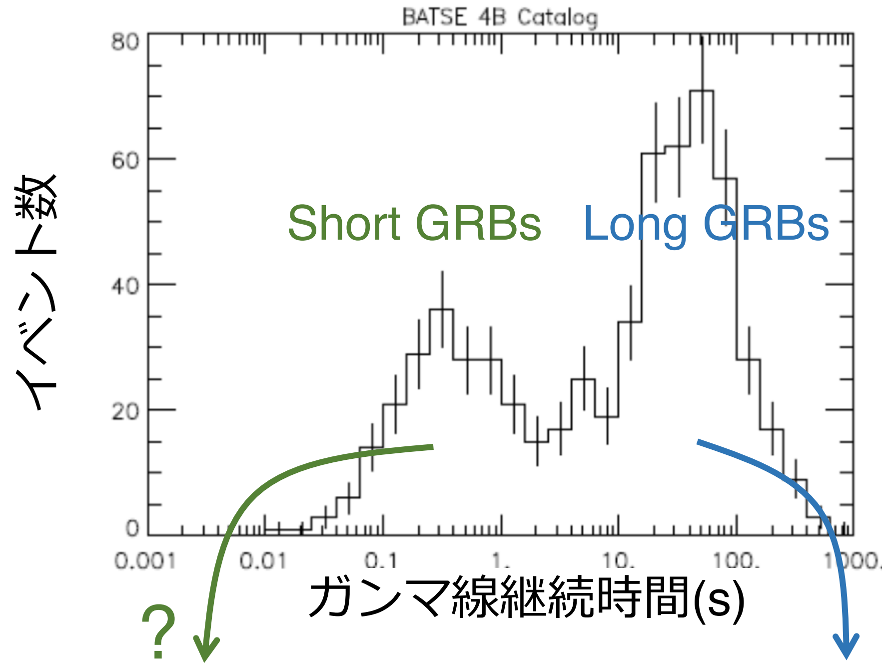

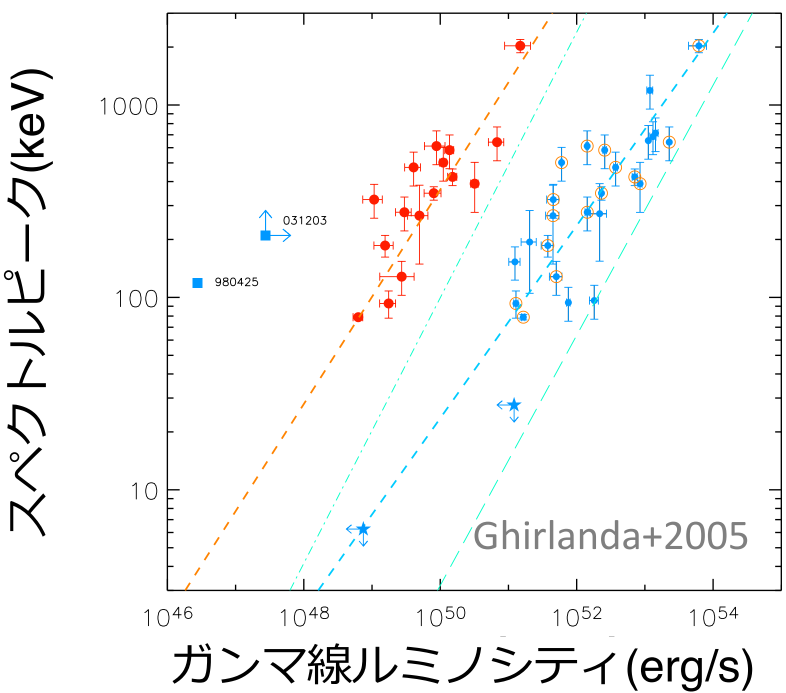

- ガンマ線の空で最も明るい現象
- 宇宙論的距離 $\langle z \rangle \sim 2$
- $\gamma > 100$

ジェットの物理の諸問題

$$L_j = \gamma \dot{M}_{\rm j} c^2 + L_{\rm th} + L_{\rm EM} \sim {\rm const.}$$

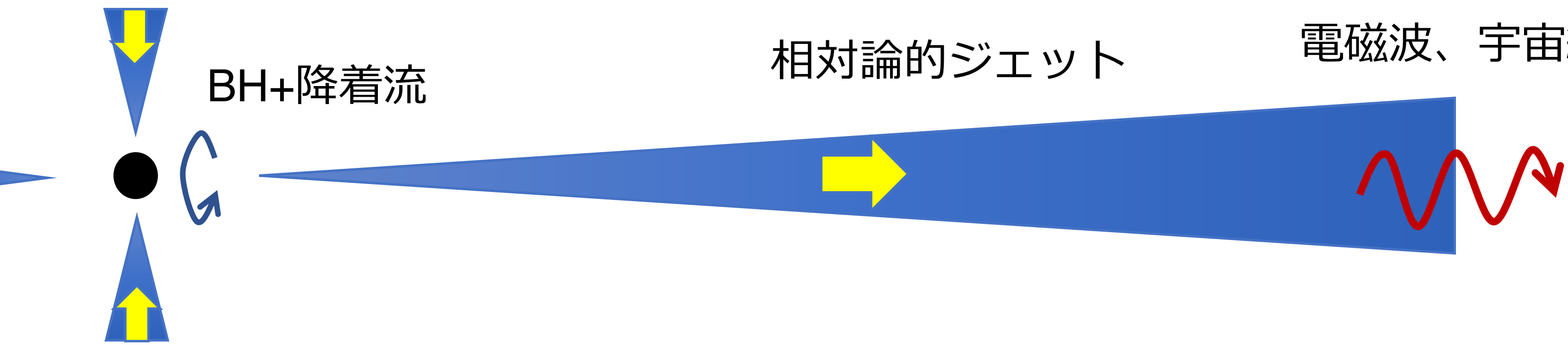

$L_{\rm j} \sim L_{\rm EM}$

or $L_{\rm th}$

$\gg \dot{M}_j c^2$

駆動機構？
粒子注入機構？

$L_{\rm EM} \to \gamma \dot{M}_{\rm j} c^2$

$L_{\rm th} \to \gamma \dot{M}_{\rm j} c^2$

加速機構？
絞り込み？

$L_{\rm EM} \to L_{\rm th}$

$\gamma \dot{M}_{\rm j} c^2 \to L_{\rm th}$

安定性？
散逸機構？
粒子加速機構？

一般相対論的電磁流体(GRMHD)シミュレーション

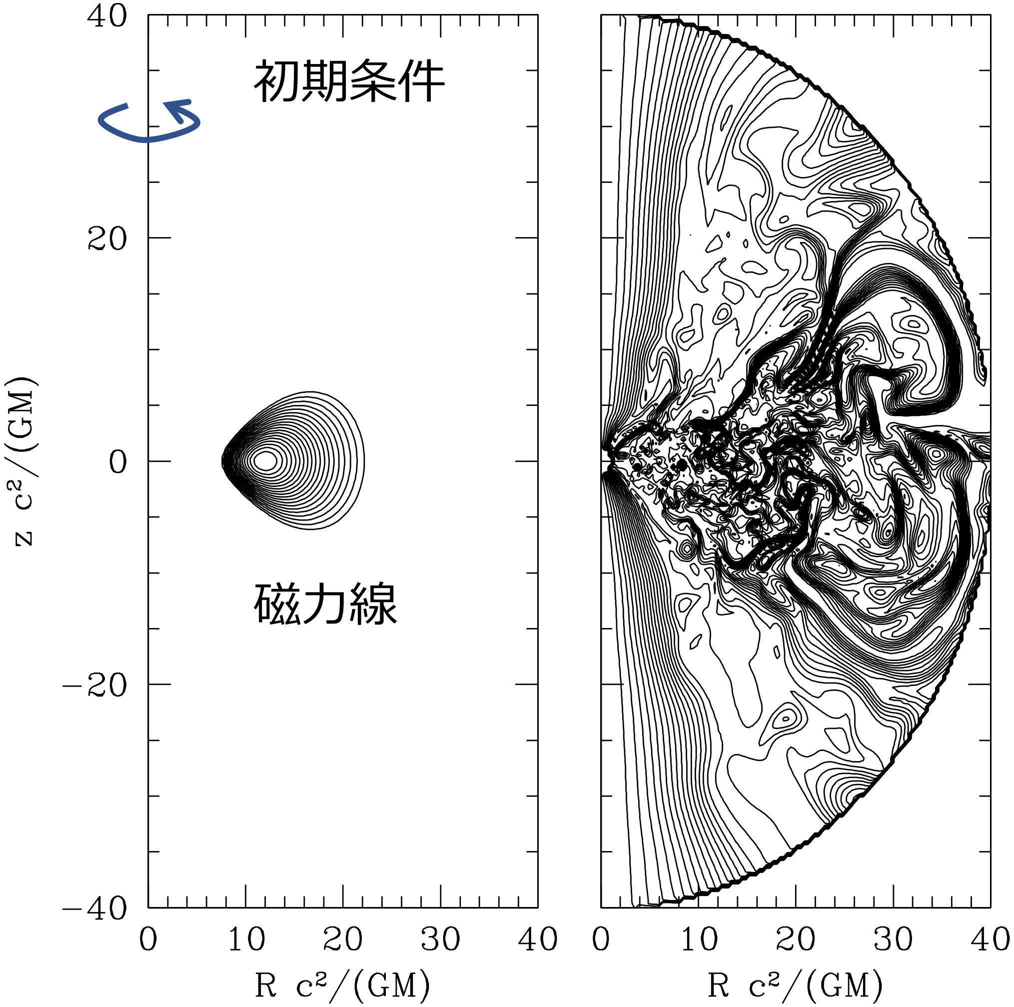

- 放射冷却が非効率で分厚い降着円盤(RIAF)
- 低密度の軸付近で相対論的速度の流れ＝ジェット

- 回転BH駆動
- MHD加速
- 外圧による絞り込み
- 人工的な粒子注入

e.g. Koide et al. 2000; Komissarov 2001; McKinney & Gammie 2004; Barkov & Komissarov 2008; Tchekhovskoy et al. 2011; Ruiz et al. 2012; Contopoulos et al. 2013

単極誘導

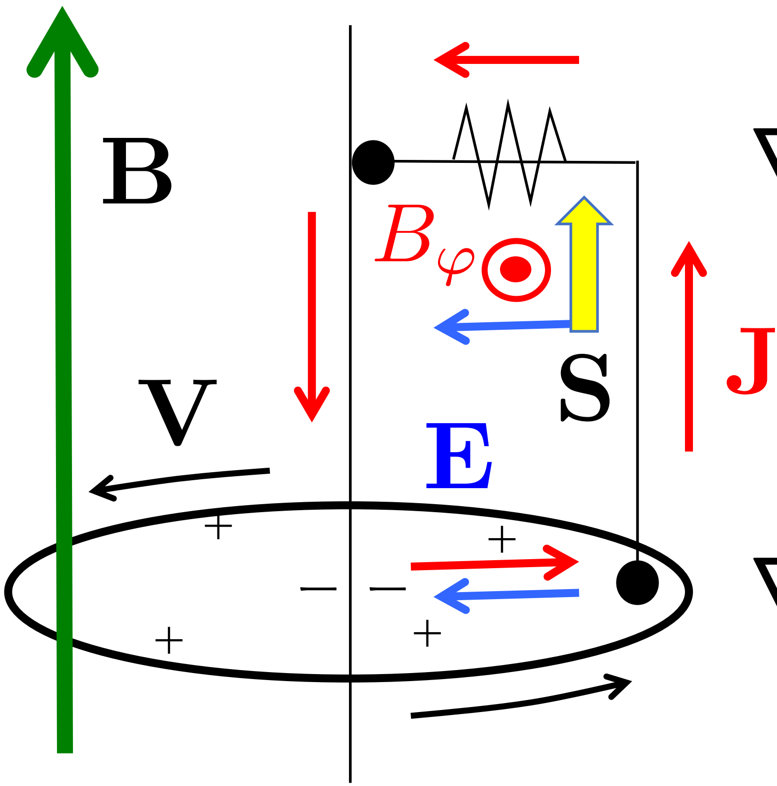

電磁エネルギーが熱に転換

$$\nabla \cdot \mathbf{S} = -\mathbf{E}\cdot\mathbf{J} < 0$$

$$\nabla \cdot \mathbf{S} = 0$$

$$\nabla \cdot \mathbf{S} = -\mathbf{E}\cdot\mathbf{J} > 0$$

円盤が回転エネルギーを失う

$$\mathbf{E} = -\frac{\mathbf{V}}{c} \times \mathbf{B}$$

- パルサー風
- 降着円盤風

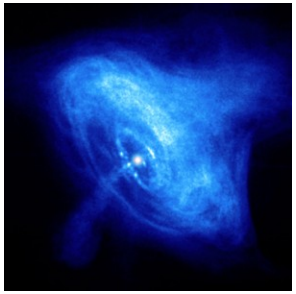

MHD加速

理想MHD（電磁流体）近似

$$\mathbf{E} + \frac{1}{c}\mathbf{V} \times \mathbf{B} = 0$$

加速： $L_{\mathrm{EM}} \to \gamma \dot{M}_{\mathrm{j}} c^2$

$$\nabla \cdot \mathbf{S}_{\mathrm{p}} = -\mathbf{E} \cdot \mathbf{J}_{\mathrm{p}}$$

$$= -\left(\frac{1}{c}\mathbf{J}_{\mathrm{p}} \times \mathbf{B}_{\varphi}\right) \cdot \mathbf{V}$$

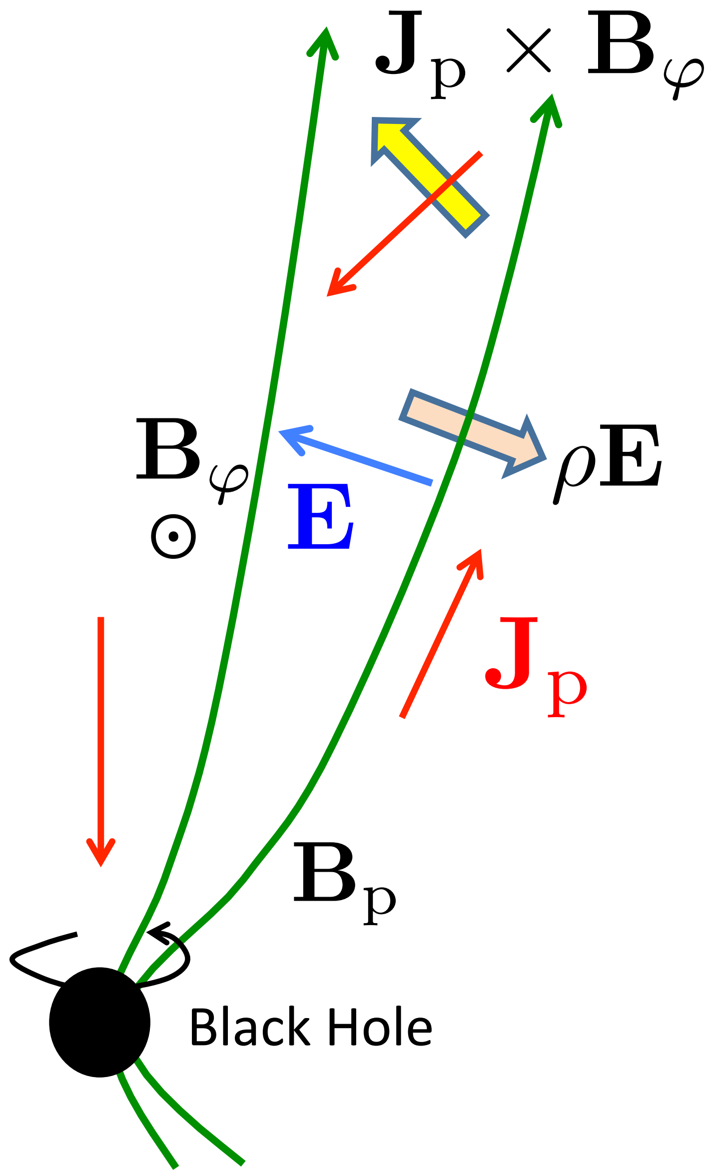

MHD加速

電流が磁力線を横切る：

$$\int \mathbf{J}_{\rm p} \cdot d\mathbf{S} = r|B_\varphi|$$

が磁力線に沿って減少

理想MHDと定常の仮定

$$|B_\varphi| \approx E = \frac{r\Omega_{\rm F}}{c} B_{\rm p}$$

磁力線に沿って$B_{\rm p}\, r^2$が減少
すれば加速する

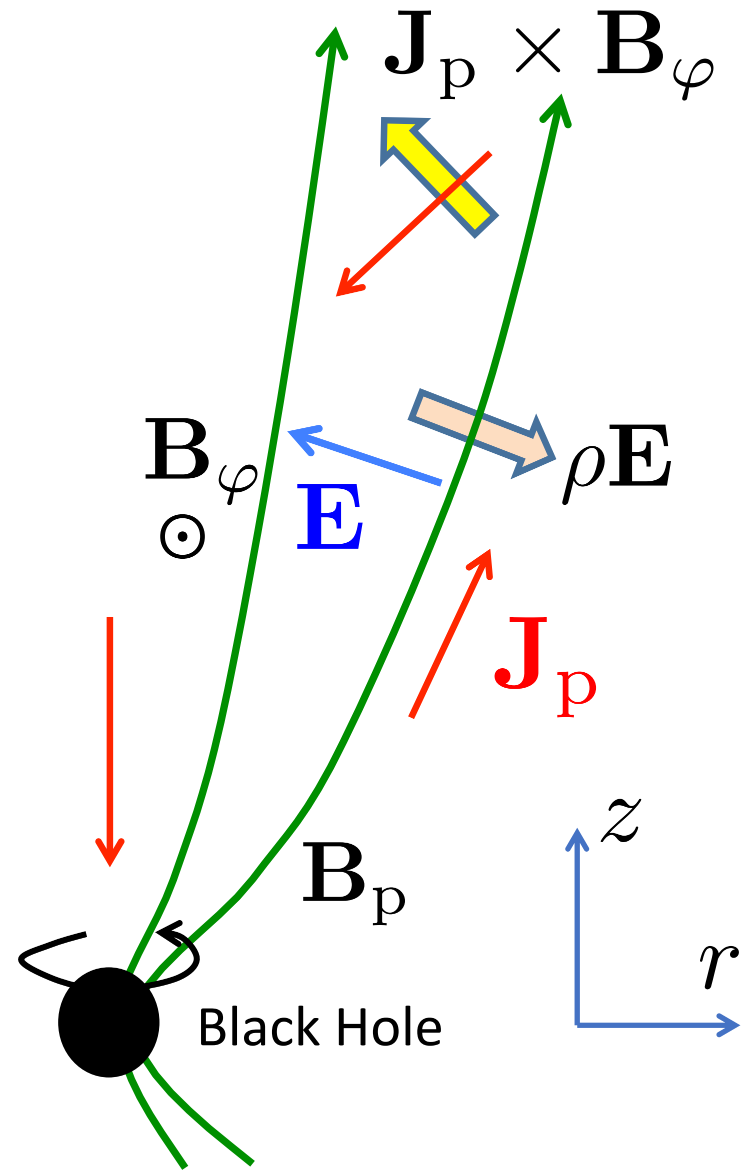

MHD加速

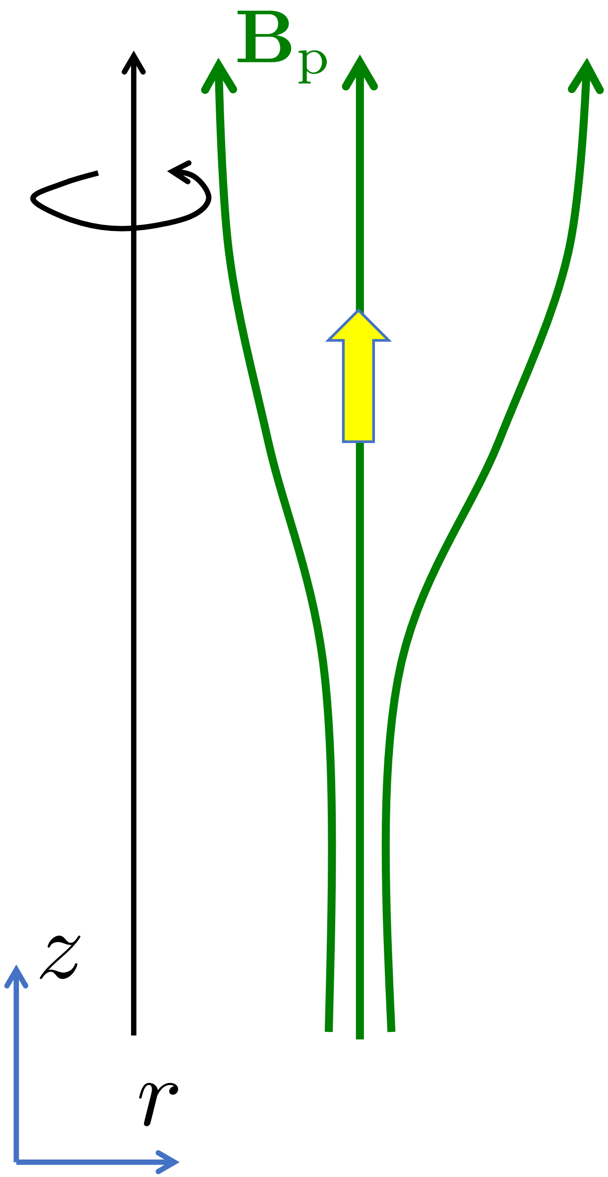

磁力線に沿って$B_{\mathrm{p}}\,r^2$が減少すれば加速する

超音速流体の振る舞いと同じ

(e.g. Begelman & Li 94; Takahashi & Shibata 98; Fendt & Ouyed 04; KT & Takahara 13)

これは亜音速流

Kerr時空

$$ds^2 = g_{\mu\nu}dx^\mu dx^\nu = -\alpha^2 dt^2 + \gamma_{ij}(\beta^i dt + dx^i)(\beta^j dt + dx^j),$$

Boyer-Lindquist座標 $a = J/(Mr_g)$

$$\alpha = \sqrt{\frac{\varrho^2\Delta}{\Sigma}}, \quad \beta^\varphi = -\frac{2ar}{\Sigma}, \quad \equiv -\Omega$$

$$\gamma_{\varphi\varphi} = \frac{\Sigma}{\varrho^2}\sin^2\theta, \quad \gamma_{rr} = \frac{\varrho^2}{\Delta}, \quad \gamma_{\theta\theta} = \varrho^2,$$

$$\varrho^2 = r^2 + a^2\cos^2\theta, \quad \Delta = r^2 + a^2 - 2r,$$
$$\Sigma = (r^2 + a^2)^2 - a^2\Delta\sin^2\theta,$$

$$r \to \infty : a \to 1, \Omega \to 0$$

$$r \to r_H : a \to 0 (\Delta \to 0)$$

座標特異点

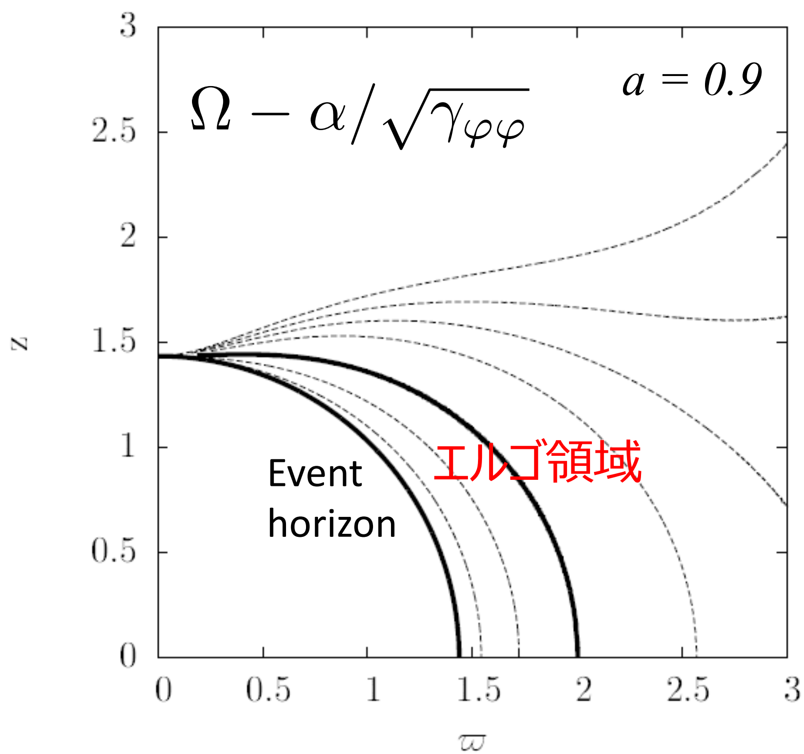

$$g_{tt} = -\alpha^2 + \gamma_{\varphi\varphi}\Omega^2 > 0$$

Cf. KT & Takahara 2014

Penrose process

$$ds^2 = g_{\mu\nu}dx^\mu dx^\nu = -\alpha^2 dt^2 + \gamma_{ij}(\beta^i dt + dx^i)(\beta^j dt + dx^j),$$

Boyer-Lindquist座標 $a = J/(Mr_g)$

$$\alpha = \sqrt{\frac{\varrho^2\Delta}{\Sigma}}, \quad \beta^\varphi = -\frac{2ar}{\Sigma}, \quad \equiv -\Omega$$

$$\gamma_{\varphi\varphi} = \frac{\Sigma}{\varrho^2}\sin^2\theta, \quad \gamma_{rr} = \frac{\varrho^2}{\Delta}, \quad \gamma_{\theta\theta} = \varrho^2,$$

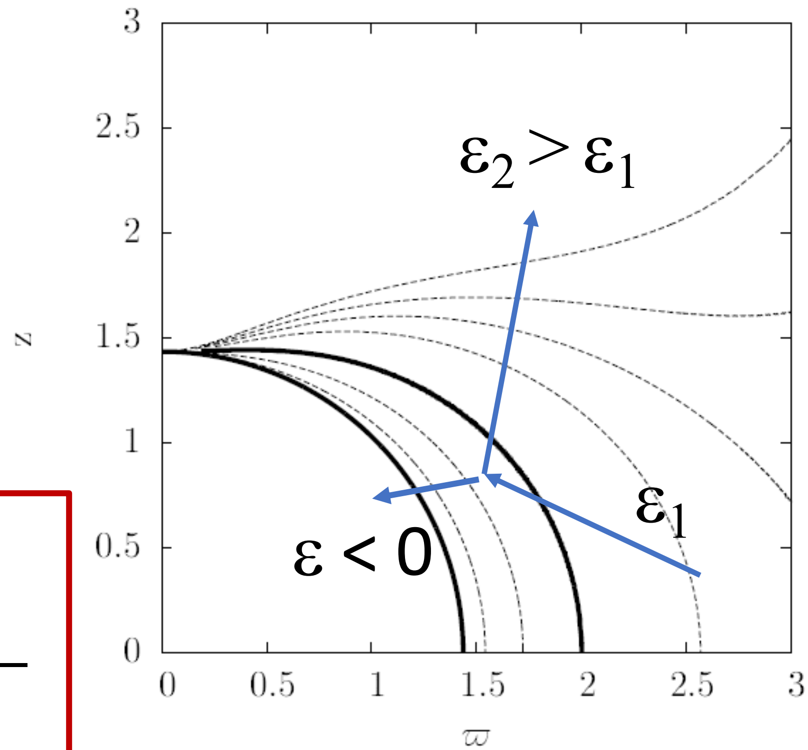

- エルゴ領域では、粒子はBHと同じ方向に回転する
- ゆっくり回転する粒子は負のエネルギー ($\varepsilon = -g_{tt}u^t\xi^t$) を持ちうる
- それを落下させるとBHのエネルギーを抽出できる（回転を減速させる）

$$g_{tt} = -\alpha^2 + \gamma_{\varphi\varphi}\Omega^2 > 0$$

Blandford-Znajek process

- Slowly rotating Kerr BH
- Steady, axisymmetric
- Split-monopole B field

- Force-free approximation (Electromagnetically dominated)

$$\nabla \cdot \mathbf{S}_{\rm p} = 0$$

Flat-space solution $H_\varphi = -2\pi\Omega_{\rm F} B^r \sqrt{\gamma}\sin\theta$

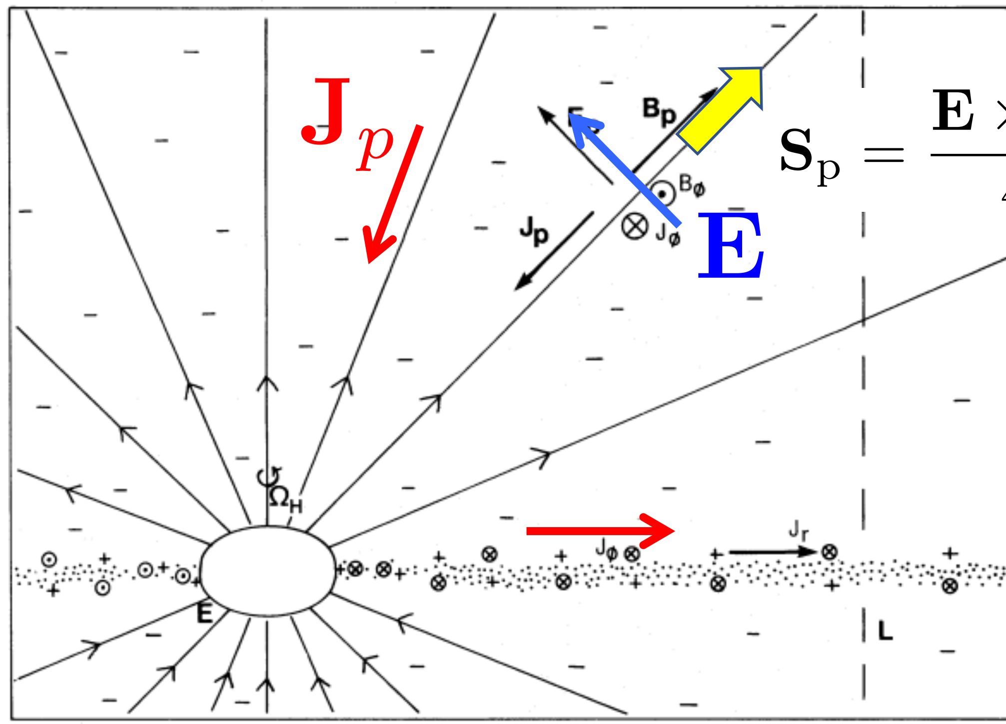

$$\mathbf{S}_{\rm p} = \frac{\mathbf{E} \times \mathbf{H}_\varphi}{4\pi}$$

$H_\varphi = 2\pi(\Omega_{\rm F} - \Omega_{\rm H}) B^r \sqrt{\gamma}\sin\theta$ Regularity at horizon

Blandford & Znajek 1977

電流はいかにして駆動されるのか？
BHはいかにしてエネルギーを失うのか？

BZ processは実際に働くのか

- Membraneパラダイム
  「地平面で電流が駆動される」？？

  K. Thorne et al. 1986; see also Okamoto 2006

- 負の電磁エネルギーが落下する？？

$$EB_\varphi c/4\pi \neq \varepsilon v$$

KT & Takahara 2016

- 定常に至る過程で電流構造が作られる

$$\nabla \cdot \mathbf{S}_p = -\partial_t e - \mathbf{E} \cdot \mathbf{J}_p$$

- 磁気張力がBHに作用する　Kinoshita & Igata 2018

- 数値シミュレーションは時空固定
- 観測で証明したい

BH時空の源は地平面の中にある

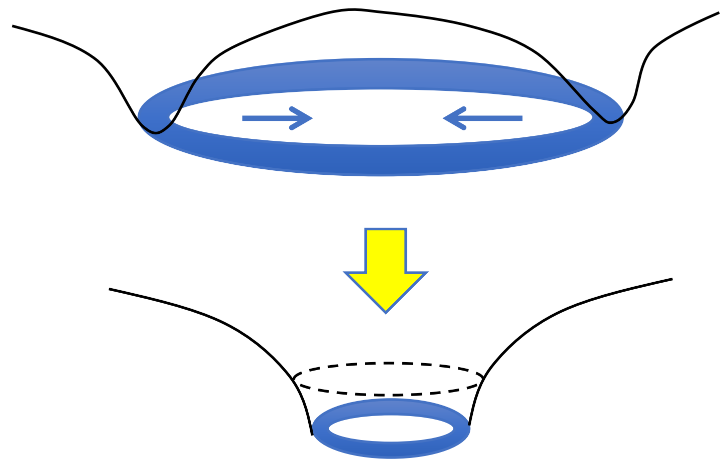

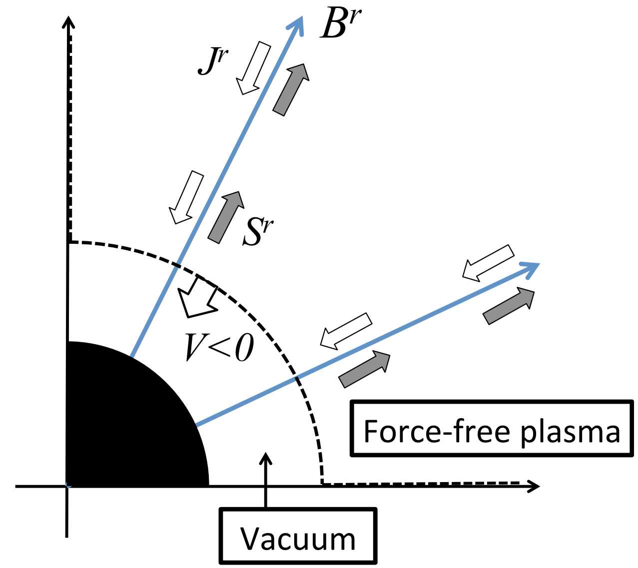

M87

- LLAGN with $L_\gamma \sim 10^{42}$ erg/s $\sim 10^{-6}\ L_{\rm Edd}$ (for $M_{\rm BH} \sim 6 \times 10^9\ M_{\rm sun}$)

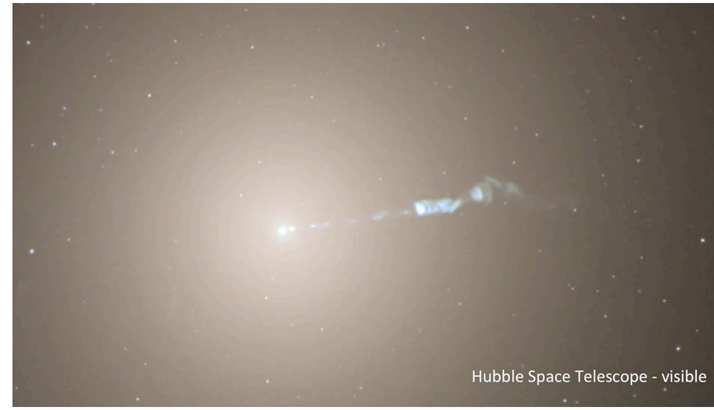

- FR-I type, but $L_{\rm j} \sim Mdot\ c^2$?
- Mechanism of a BH jet / accretion disk

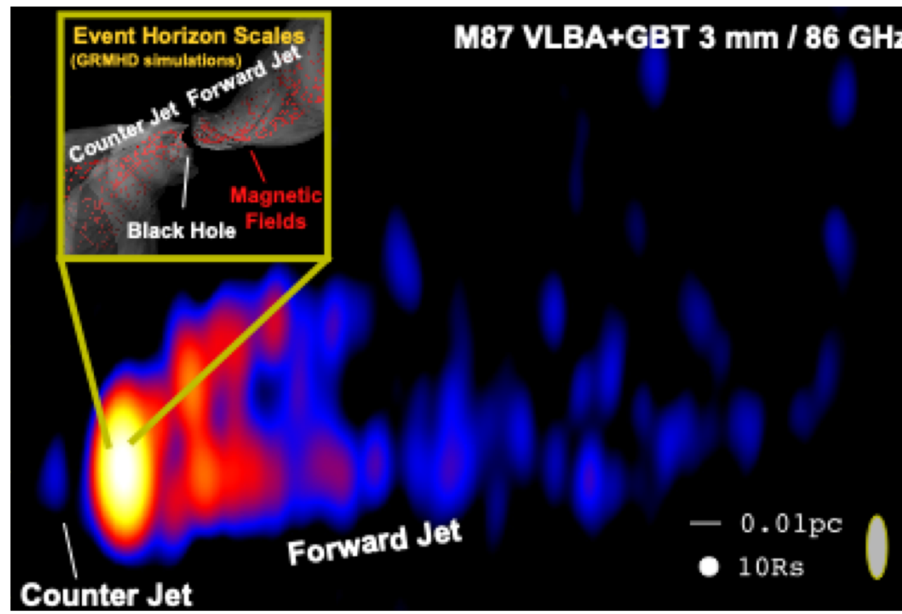

Hada+2016

- Imaging of a black hole shadow
  - Test of GR
  - BH as a central engine of AGN

86 GHz (3.5mm); VLBA+GBT

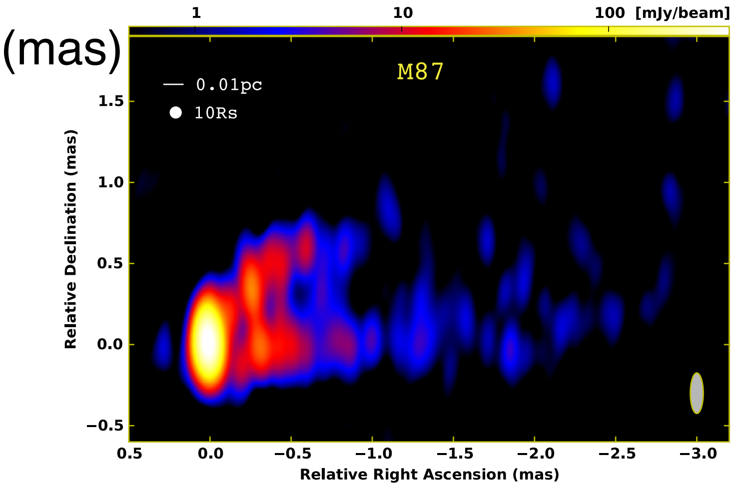

15 GHz; VLBA+VLA

(VSOP also detected the triple-ridge)

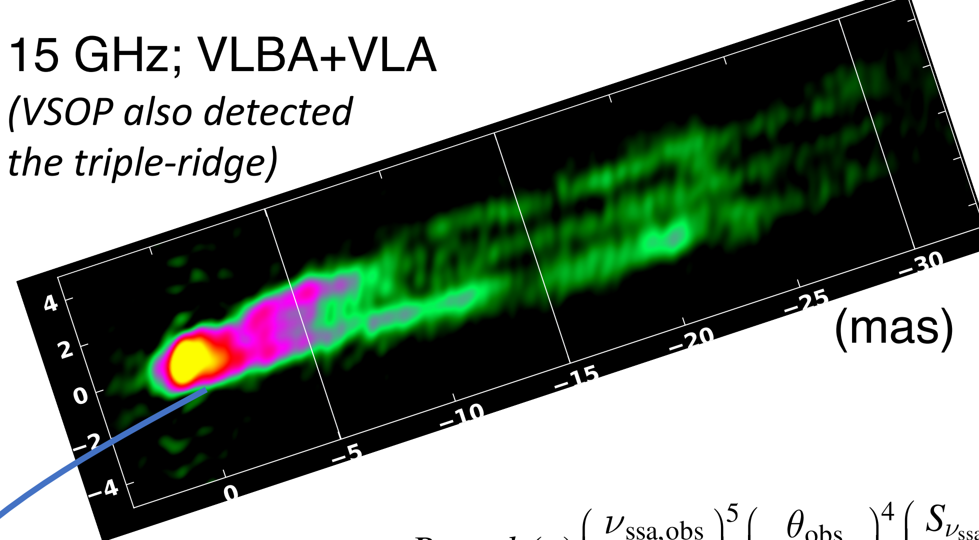

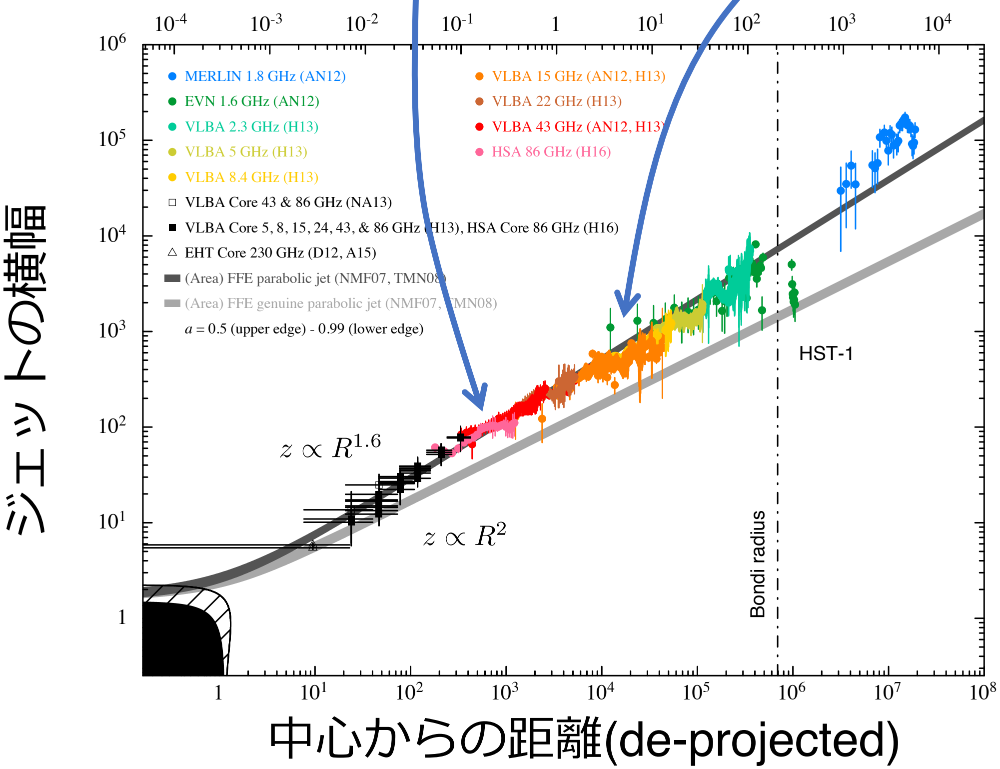

$$B_\perp = b(p)\left(\frac{\nu_{\mathrm{ssa,obs}}}{1\ \mathrm{GHz}}\right)^5\left(\frac{\theta_{\mathrm{obs}}}{1\ \mathrm{mas}}\right)^4\left(\frac{S_{\nu_{\mathrm{ssa,obs}}}}{1\ \mathrm{Jy}}\right)^{-2} \times \left(\frac{\delta}{1+z}\right),$$

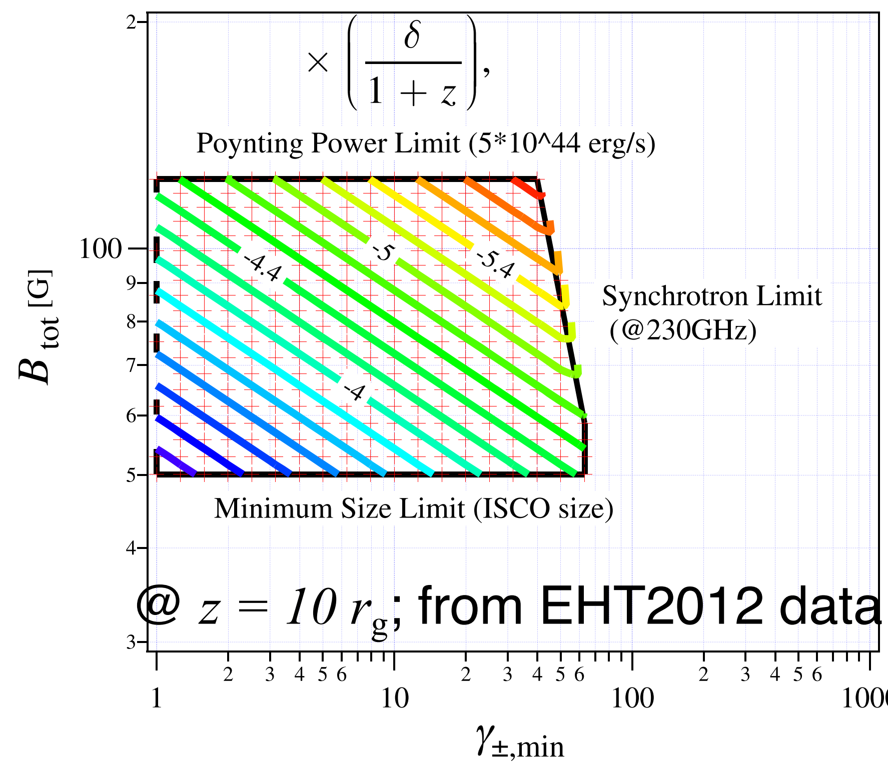

@ $z = 10\ r_g$; from EHT2012 data

Asada & Nakamura 2012; Hada+2013, 2016, 2017; Nakamura+2018; Kino+2015

The Event Horizon Telescope Collaboration
Kazunori Akiyama[1,2,3,4], Antxon Alberdi[5], Walter Alef[6], Keiichi Asada[7], Rebecca Azulay[8,9,6], Anne-Kathrin Baczko[6], David Ball[10], Mislav Baloković[4,11], John Barrett[2], Dan Bintley[12], Lindy Blackburn[4,11], Wilfred Boland[13], Katherine L. Bouman[4,11,14], Geoffrey C. Bower[15], Michael Bremer[16], Christiaan D. Brinkerink[17], Roger Brissenden[4,11], Silke Britzen[6], Avery E. Broderick[18,19,20], Dominique Broguiere[16], Thomas Bronzwaer[17], Do-Young Byun[21,22], John E. Carlstrom[23,24,25,26], Andrew Chael[4,11], Chi-kwan Chan[10,27], Shami Chatterjee[28], Koushik Chatterjee[29], Ming-Tang Chen[15], Yongjun Chen (陈永军)[30,31], Ilje Cho[21,22], Pierre Christian[10,11], John E. Conway[32], James M. Cordes[28], Geoffrey B. Crew[2], Yuzhu Cui[33,34], Jordy Davelaar[17], Mariafelicia De Laurentis[35,36,37], Roger Deane[38,39], Jessica Dempsey[12], Gregory Desvignes[6], Jason Dexter[40], Sheperd S. Doeleman[4,11], Ralph P. Eatough[6], Heino Falcke[17], Vincent L. Fish[2], Ed Fomalont[1], Raquel Fraga-Encinas[17], Per Friberg[12], Christian M. Fromm[36], José L. Gómez[5], Peter Galison[1,41,42], Charles F. Gammie[43,44], Roberto García[16], Olivier Gentaz[16], Boris Georgiev[19,20], Ciriaco Goddi[17,45], Roman Gold[36], Minfeng Gu (顾敏峰)[30,46], Mark Gurwell[11], Kazuhiro Hada[33,34], Michael H. Hecht[2], Ronald Hesper[47], Luis C. Ho (何子山)[48,49], Paul Ho[7], Mareki Honma[33,34], Chih-Wei L. Huang[7], Lei Huang (黄磊)[30,46], David H. Hughes[50], Shiro Ikeda[3,51,52,53], Makoto Inoue[7], Sara Issaoun[17], David J. James[4,11], Buell T. Jannuzi[10],

Bart Ripperda, Freek Roelofs, Alan Rogers, Eduardo Ros, Mel Rose, Arash Roshanineshat, Helge Rottmann,
Alan L. Roy[6], Chet Ruszczyk[2], Benjamin R. Ryan[80,81], Kazi L. J. Rygl[63], Salvador Sánchez[82], David Sánchez-Arguelles[50,83], Mahito Sasada[33,84], Tuomas Savolainen[6,85,86], F. Peter Schloerb[74], Karl-Friedrich Schuster[16], Lijing Shao[6,49], Zhiqiang Shen (沈志强)[30,31], Des Small[56], Bong Won Sohn[21,22,87], Jason SooHoo[2], Fumie Tazaki[33], Paul Tiede[19,20], Remo P. J. Tilanus[17,45,88], Michael Titus[2], Kenji Toma[89,90], Pablo Torne[6,82], Tyler Trent[10], Sascha Trippe[91], Shuichiro Tsuda[33], Ilse van Bemmel[56], Huib Jan van Langevelde[56,92], Daniel R. van Rossum[17], Jan Wagner[6], John Wardle[93], Jonathan Weintroub[4,11], Norbert Wex[6], Robert Wharton[6], Maciek Wielgus[4,11], George N. Wong[43], Qingwen Wu (吴庆文)[94], André Young[17], Ken Young[11], Ziri Younsi[95,36], Feng Yuan (袁峰)[30,46,96], Ye-Fei Yuan (袁业飞)[97], J. Anton Zensus[6], Guangyao Zhao[21], Shan-Shan Zhao[17,61], Ziyan Zhu[42], Jadyn Anczarski[98], Frederick K. Baganoff[99], Andreas Eckart[6,100], Joseph R. Farah[11,101,4], Daryl Haggard[102,103,104], Zheng Meyer-Zhao[7,105], Daniel Michalik[106,107], Andrew Nadolski[44], Joseph Neilsen[98], Hiroaki Nishioka[7], Michael A. Nowak[108], Nicolas Pradel[7], Rurik A. Primiani[109], Kamal Souccar[74], Laura Vertatschitsch[11,109], Paul Yamaguchi[11], and Shuo Zhang[99]

EHT images

- Central depression in brightness with a flux ratio >~ 10:1
- Ring shape
  - no extended component (jet / accretion disk) -> EHT 2020
- Flux ~ 0.5 Jy
- Asymmetry
- Stable in different days

$$F_\nu \simeq 0.5 \text{ Jy} \times \left(\frac{\theta}{40\mu as}\right)^2 \left(\frac{\nu}{230\text{GHz}}\right)^2 \frac{T_b}{6 \times 10^9\text{K}}$$

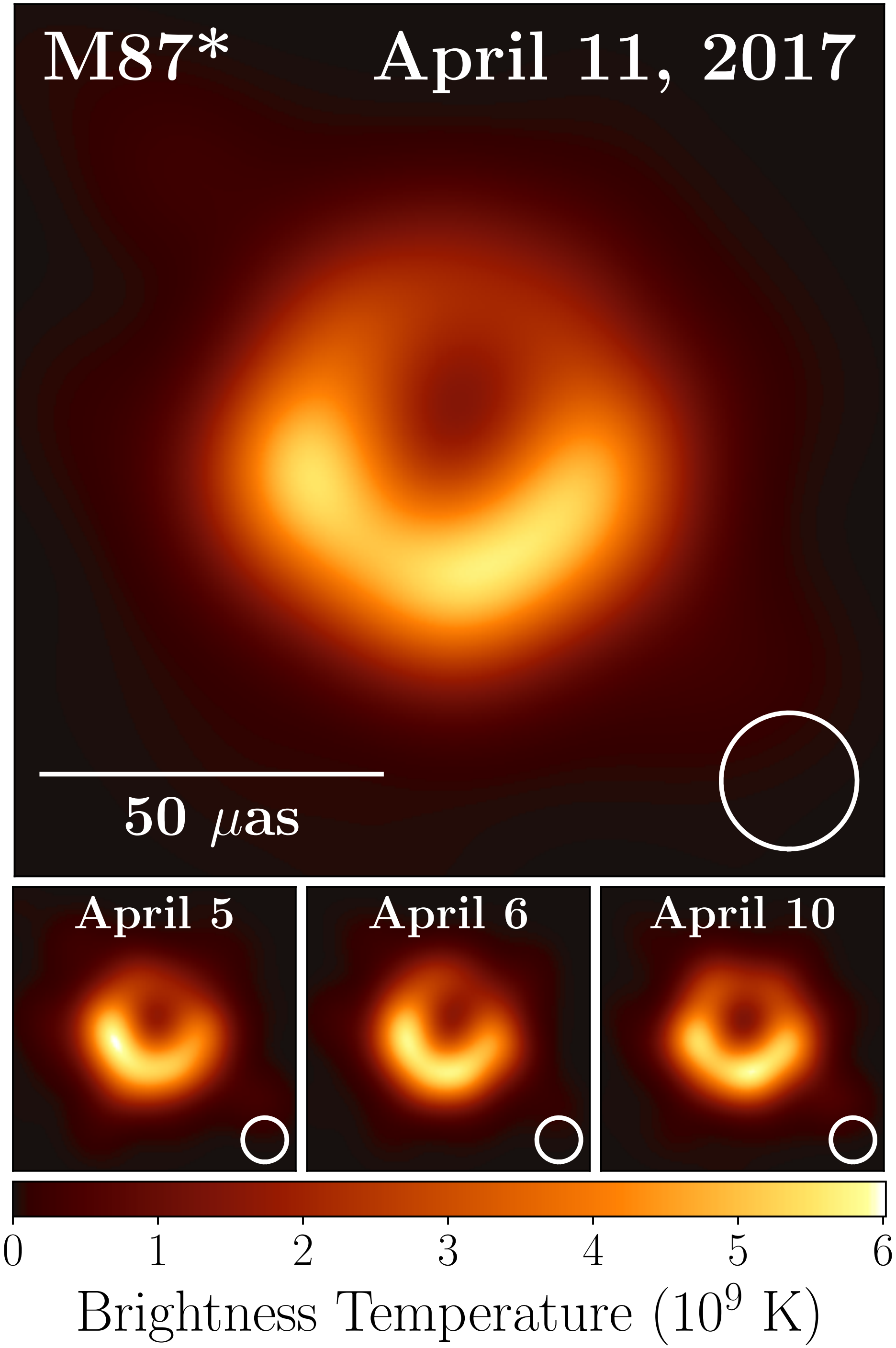

Black hole shadow & photon ring

Zero-spin BH with emitting plane

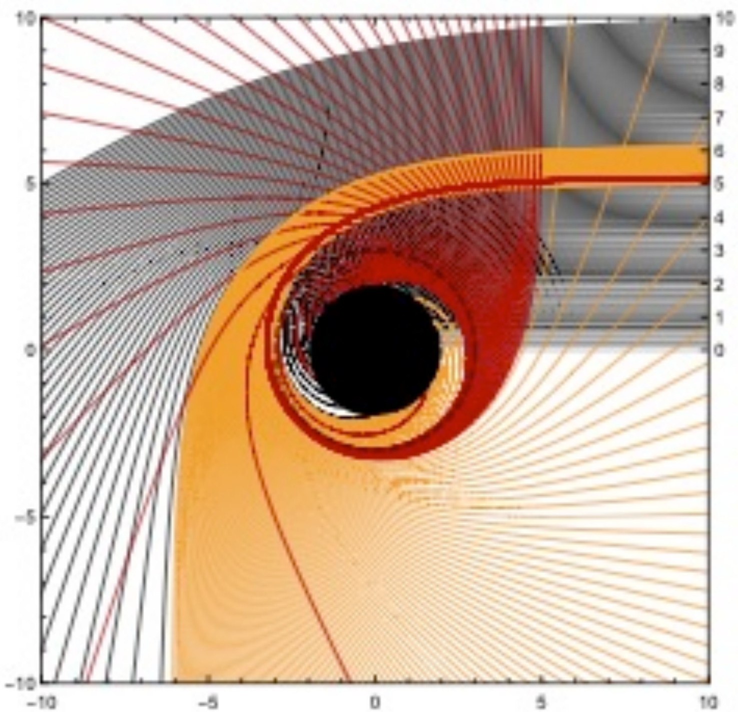

$3\sqrt{3}\ r_g$

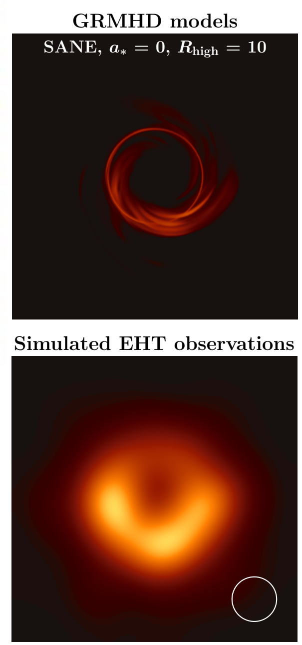

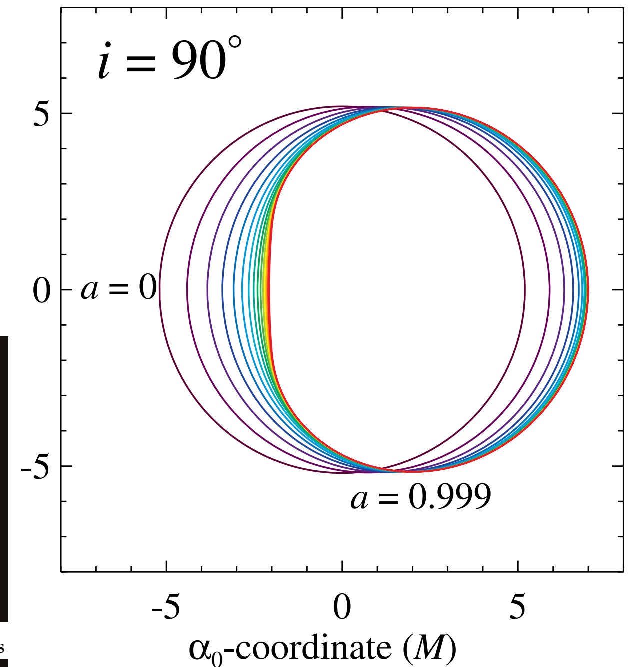

- 光子の不安定軌道(r = 3 r_g)の近くを通る光線が際立って明るく観測される

- シャドウの形はBHスピンに強く依存しない

Gralla, Holz & Wald 2019

R. Takahashi 2004; Chan, Psaltis & Ozel 2013; Pu+2016

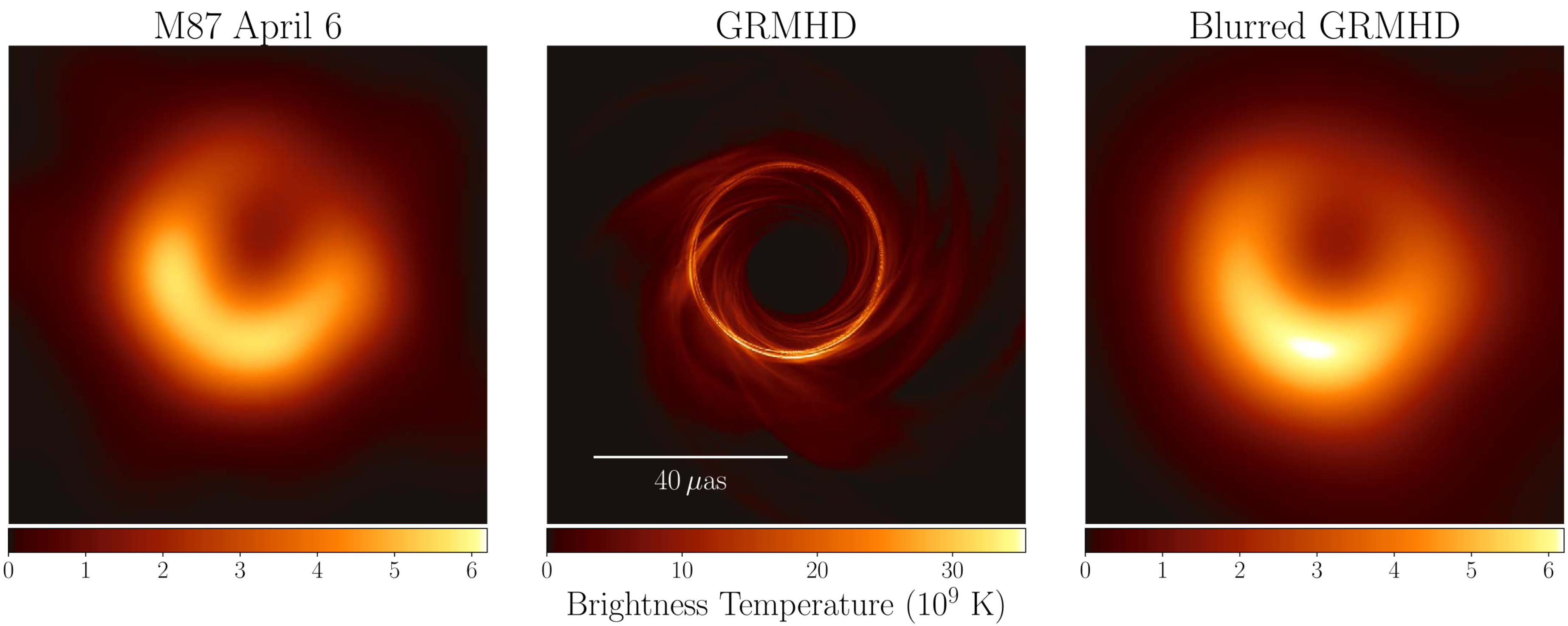

Figure 1. Left panel: an EHT2017 image of M87 from Paper IV of this series (see their Figure 15). Middle panel: a simulated image based on a GRMHD model. Right panel: the model image convolved with a 20 μas FWHM Gaussian beam. Although the most evident features of the model and data are similar, fine features in the model are not resolved by EHT.

GRMHD + GRRT calculations

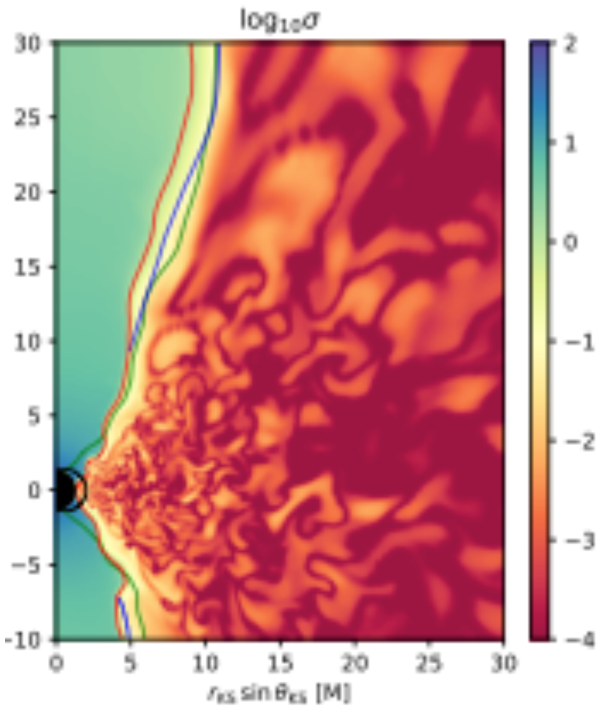

Porth+ 2019

- BH spin: a_* = -0.94, -0.5, 0, 0.5, 0.75, 0.97 & more
- r <~ 10 rgで準定常状態
- BHを貫く磁束　$\phi \equiv \Phi_{\rm BH}(\dot{M} r_{\rm g}^2\ c)^{-1/2}$
  SANE models (ϕ ~ 3), MAD models (ϕ > 50)

- 電子温度のパラメータ $R_{\rm high}$

$$R \equiv \frac{T_i}{T_e} = R_{\rm high}\frac{\beta_{\rm p}^2}{1+\beta_{\rm p}^2} + \frac{1}{1+\beta_{\rm p}^2}$$

- Funnel領域は光らせない
- inclination i = 12°, 17°, 22°, 158°, 163°, 168°

- 残るパラメータは$M_{\rm BH}$と$M_{\rm torus}$
  （長さスケールと明るさの絶対値を決める）

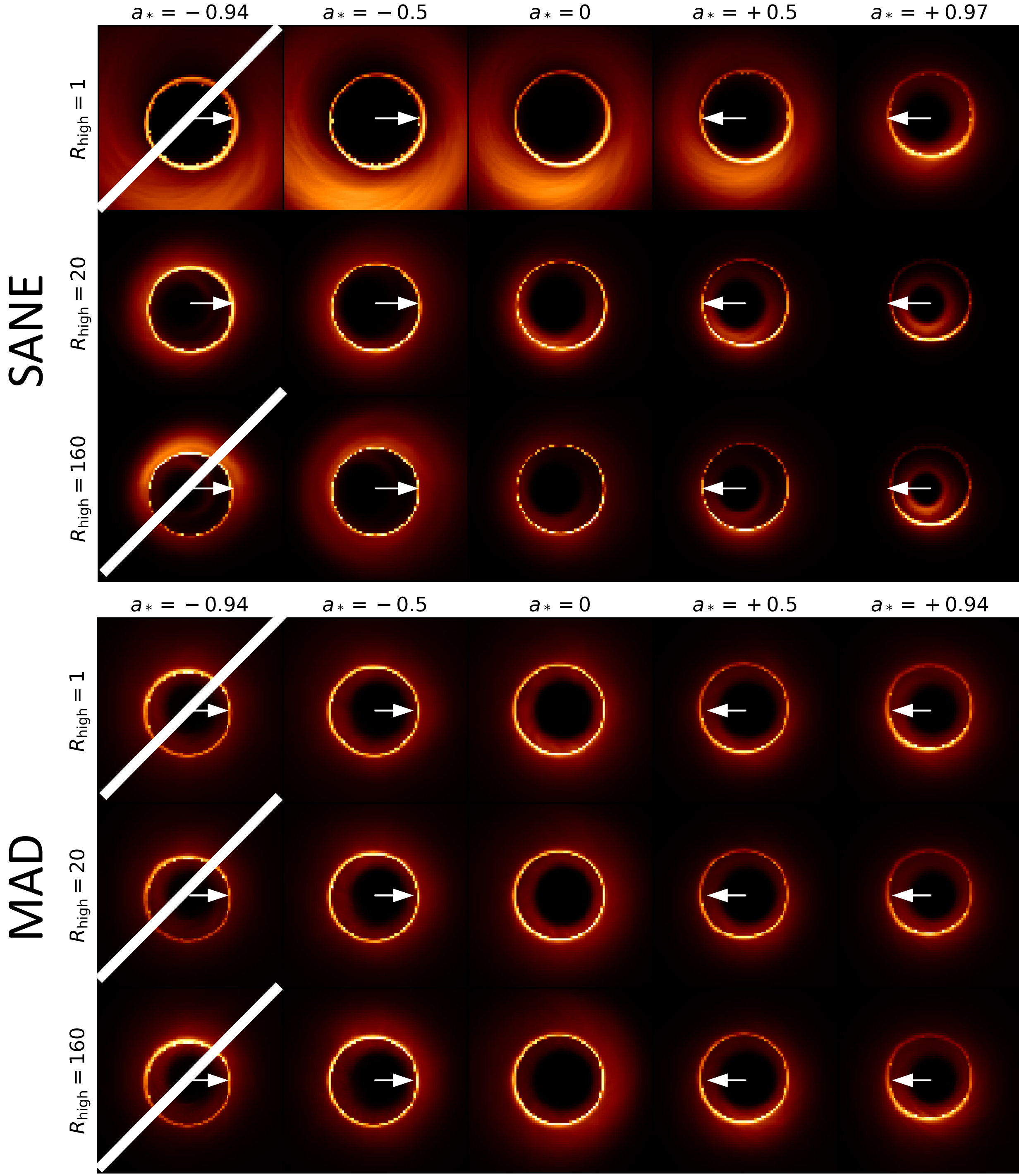

inclination i = 163°

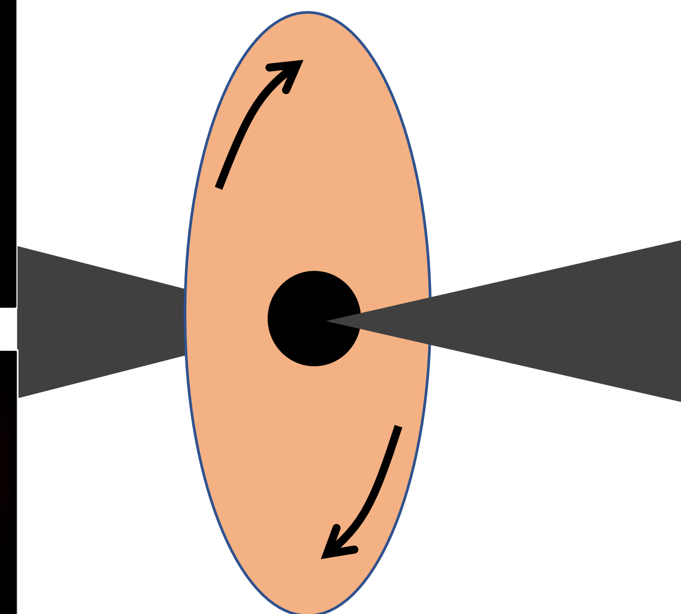

- 白矢印はBHスピンベクトル（を天空面に射影）。それが非対称性を決める

EHT観測データの理論解釈

- データは次の仮説と整合的である
  - 1.3mm放射はKerr時空の数rg以内で生じている
  - RIAFの熱的電子のoptically-thin シンクロトロン放射
  - BHによる強い重力レンズ効果＋特殊相対論的ビーミング
- 観測されたリングは、降着プラズマの性質にあまり依存せず再現される
- 一般相対論の検証、SMBHの存在の確定
- $M = 6.5^{+0.7}_{-0.6} \times 10^9 M_{sun}$ ($M/D = 3.8^{+0.4}_{-0.3}$ μas). これは以前の星の運動の観測による推定と整合的
- BHのスピンの制限はできなかった
- ジェットの方向はこれまでの観測と約90°ズレている

Ongoing work

- Polarization: further constraints on n_e, B
- Combination of EHT data and lower freq. VLBI data
  (Nakamura+18; Chael+19; Kino+14, 15; K. Takahashi+18)
- EHT 2020: more stations
  - imaging extended component
  - time variability?
- Future EHT 345 GHz campaigns
  - Green Land Telescope constructed by ASIAA, Taiwan
  - Lower optical depth & higher spatial resolution
    -> Kawashima+2019; Nakamura+2019 in prep.

Connection of the ring with the jet

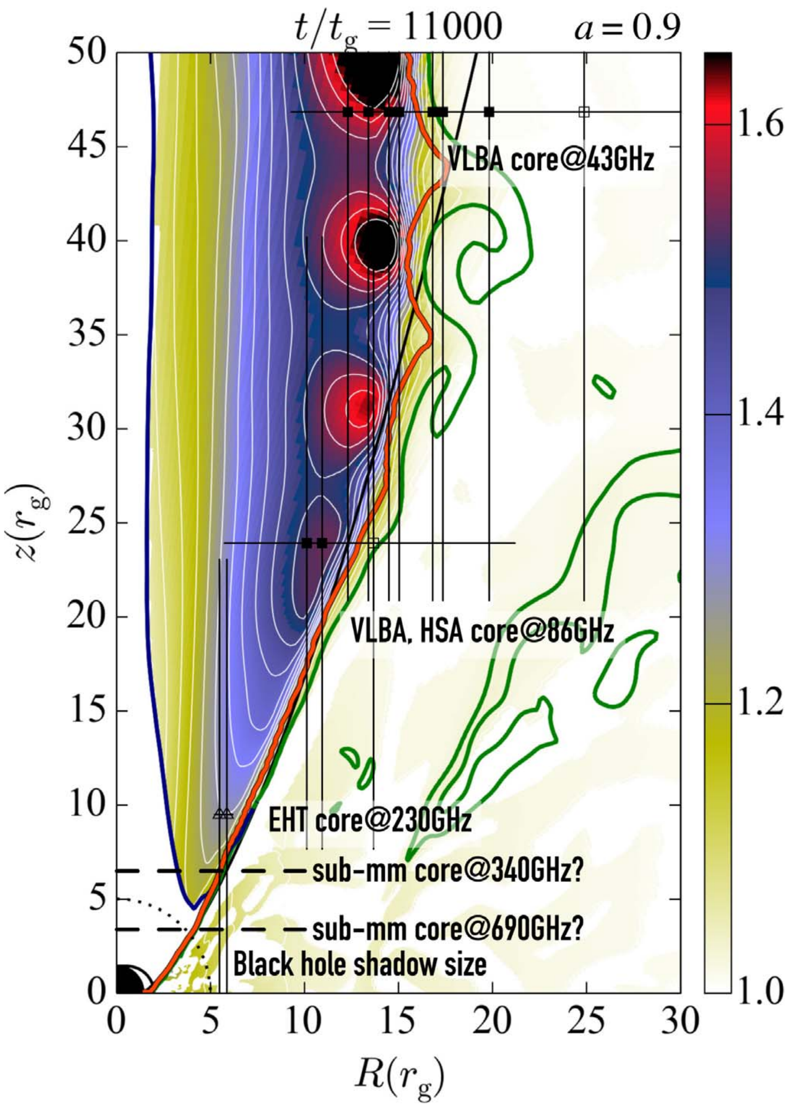

Nakamura+2018

- BZ processの観測的証拠は得られるか？

□ 相対論的ジェットの最上流イメージング

□ $P_{BZ} = P_{BZ}(a_*, \Phi_{BH})$

□ 他の間接的証拠を集める

- Stagnation surface
- Blob formation found in 2D high resolution simulations
- The most upstream of blobs may not be the stagnation surface
- But MHD simulations do not include pair-creation gaps

Large-scale jet emission model

$$\Psi = Ar^{\nu}(1 \mp \cos\theta)$$

Consistent with numerical FF simulations

$$\mathbf{B}_p = \frac{1}{R}\nabla\Psi \times \hat{\phi}, \quad B_\phi = \mp\frac{2\Psi\Omega}{Rc}$$

cf. Tchekhovskoy+2008

$$\mathbf{E} = -\frac{1}{c}\Omega\nabla\Psi = -\frac{R\Omega}{c}\hat{\phi}\times\mathbf{B}$$

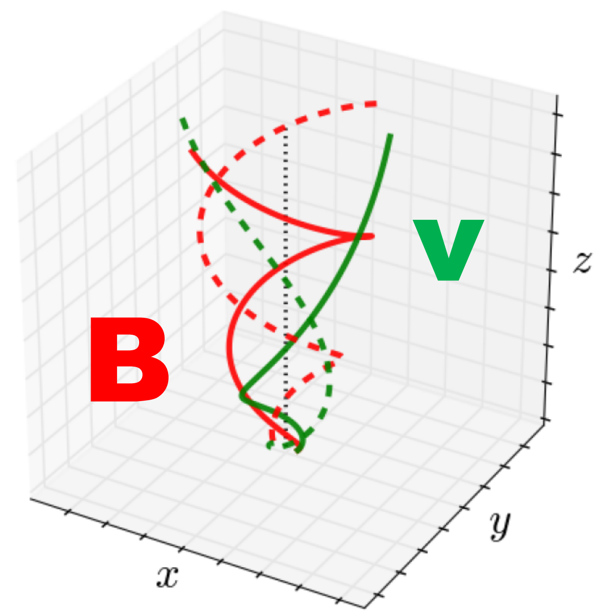

$$\mathbf{v} = \frac{\mathbf{E}\times\mathbf{B}}{B^2}c,$$

Approaching MHD velocity at far zone

$$\nabla\cdot(n\mathbf{v}) = 0$$

K. Takahashi, KT, Kino, M. Nakamura & Hada 2018

BP type: 降着円盤駆動モデル

$$\Omega = \Omega_{\mathrm{Kep}} = \sqrt{\frac{GM}{R^3}}$$

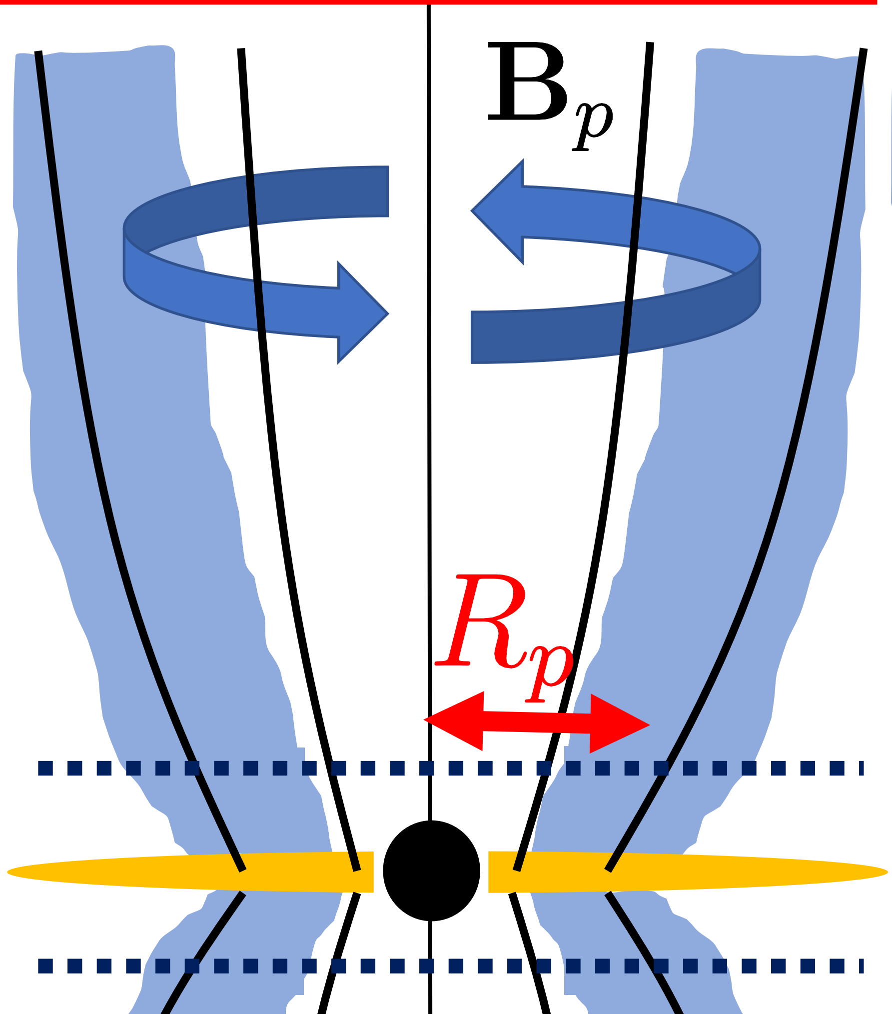

BZ type: BH駆動モデル

$$\Omega = \frac{1}{2}\Omega_{\mathrm{BH}} = \mathrm{const.}$$

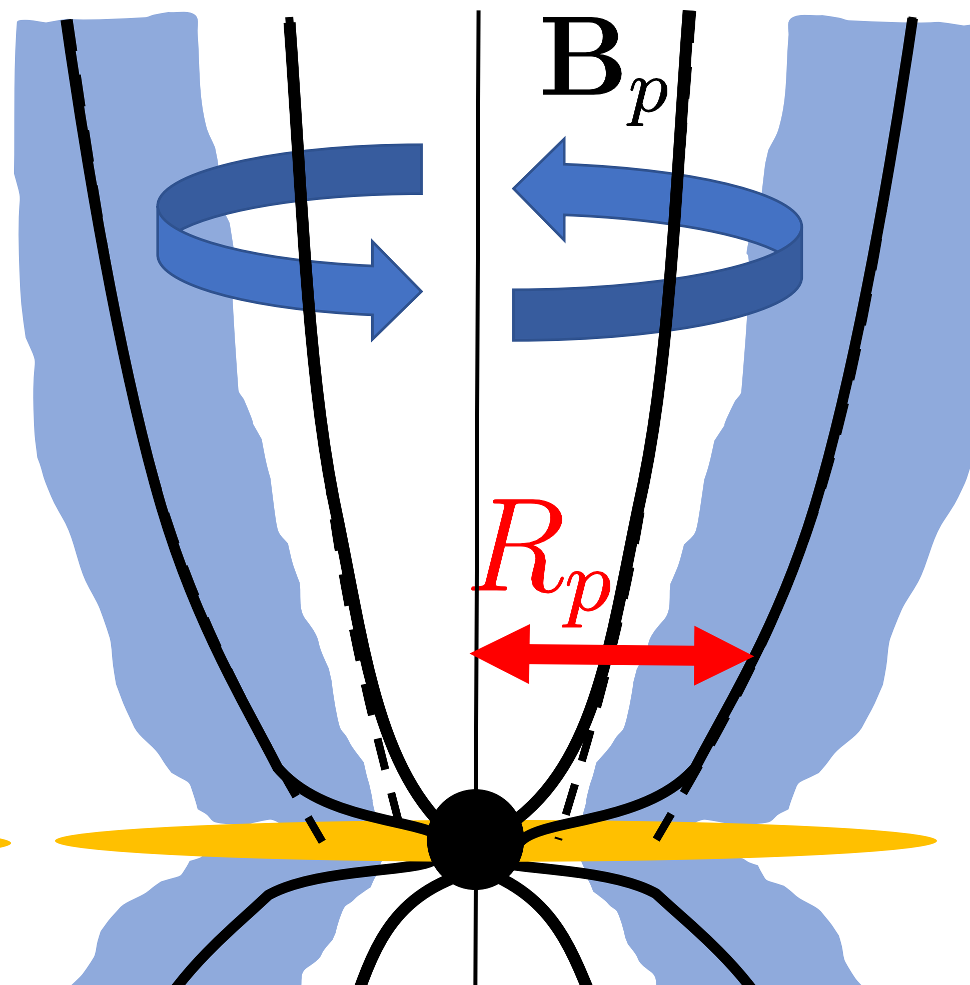

BP type: 降着円盤駆動モデル

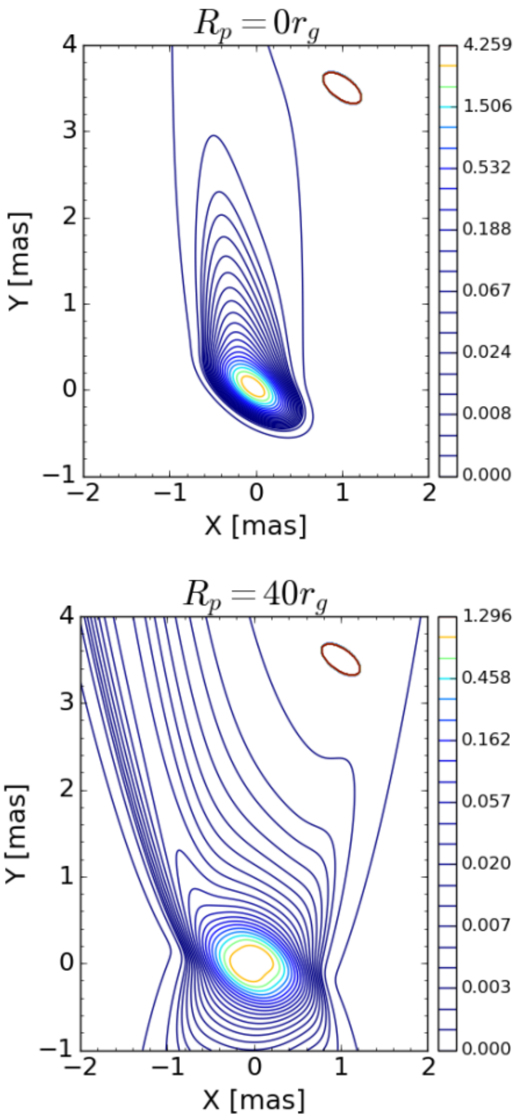

回転が遅いと加速が遅く、
v_ϕが大きく非対称になる

BZ type: BH駆動モデル

$a = 0.1$ $a = 0.998$

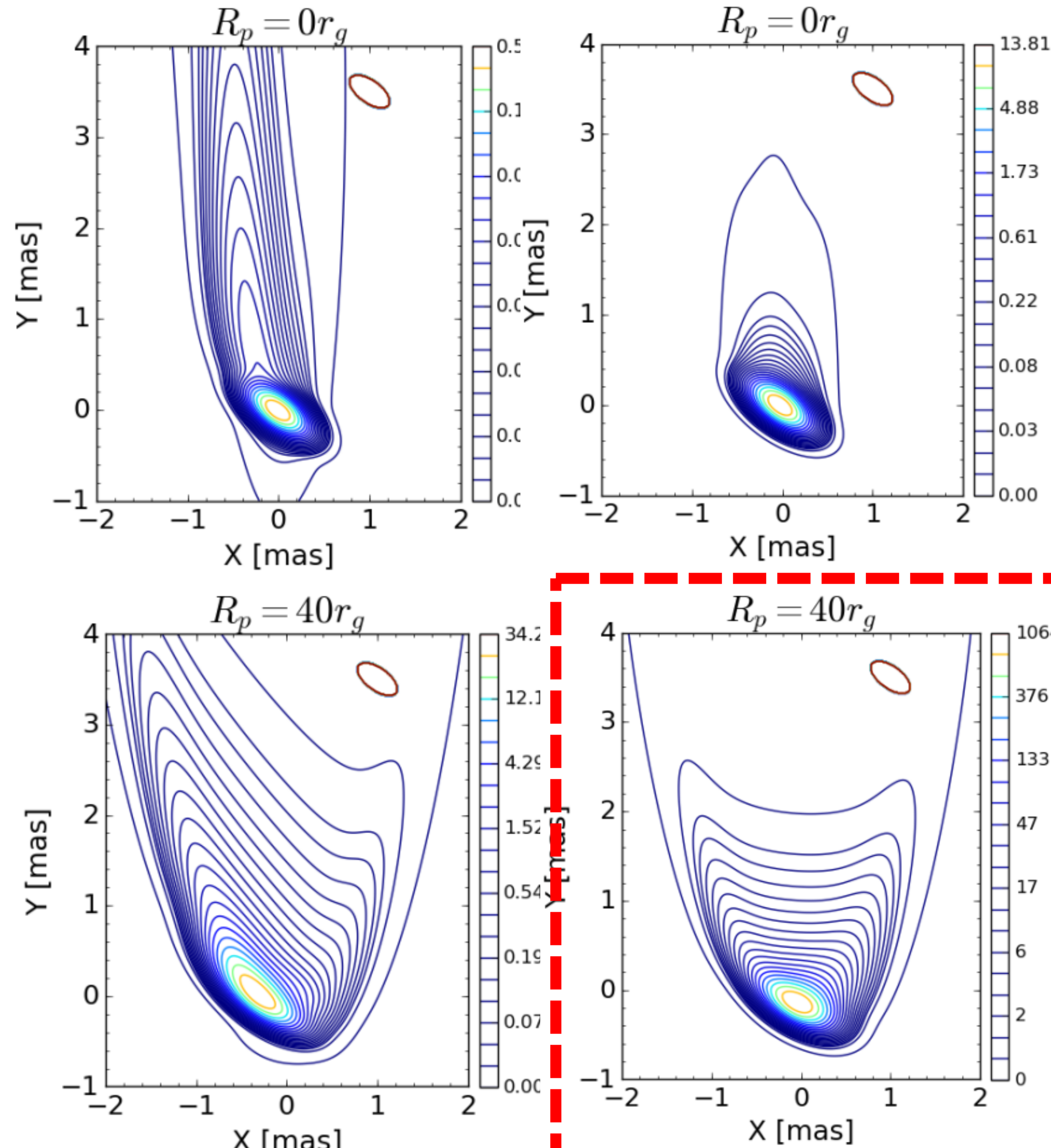

Triple-ridge image

15 GHz; VLBA+VLA

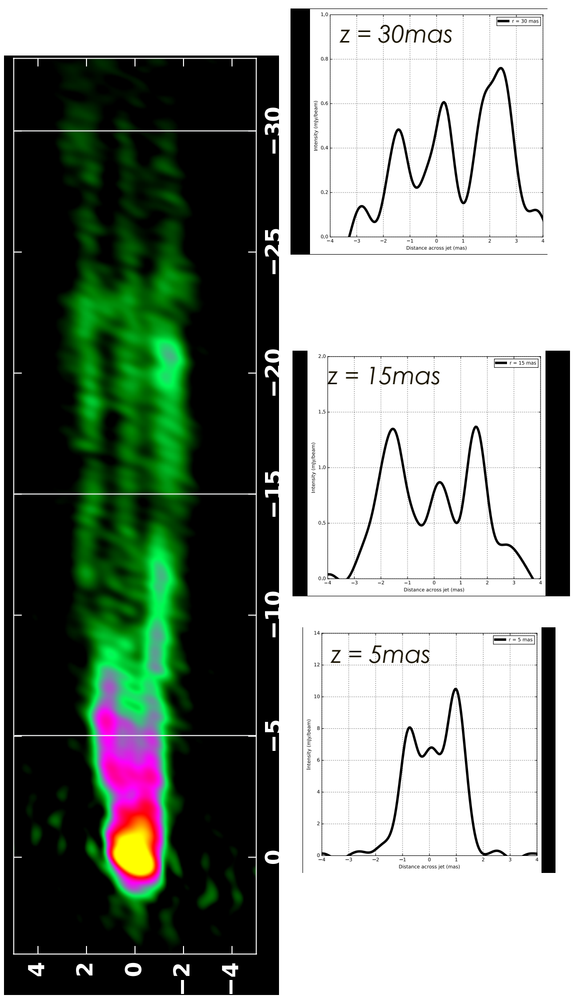

Hada et al. 2017

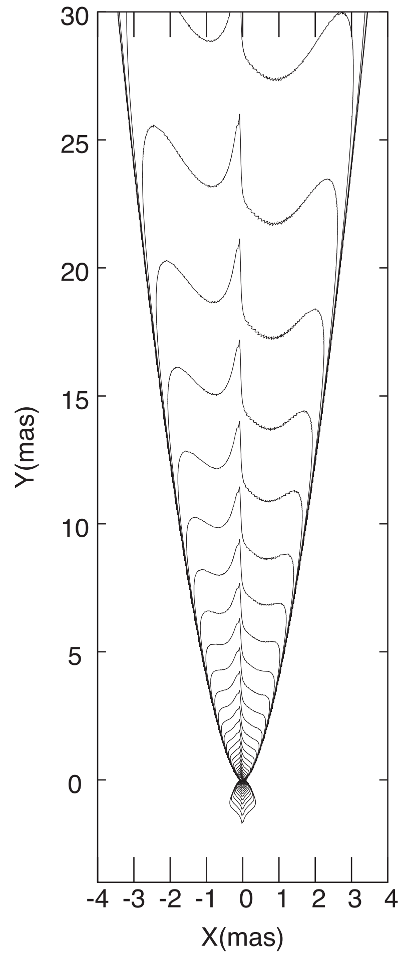

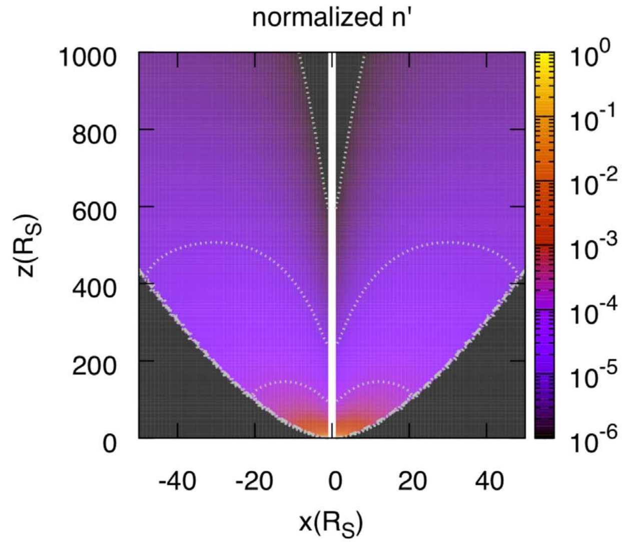

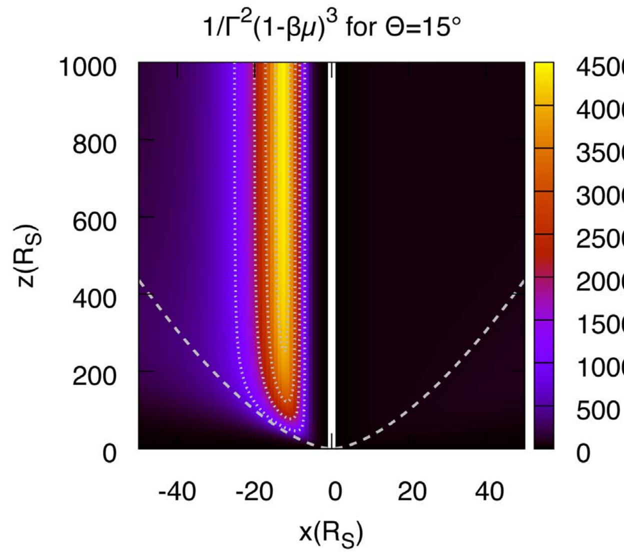

- 軸集中粒子分布
- 軸付近は密度も磁場も小さいがビーミング効果で明るくなる

Ogihara, K. Takahashi, & KT 2019

GMVA + ALMA 2020 forecast

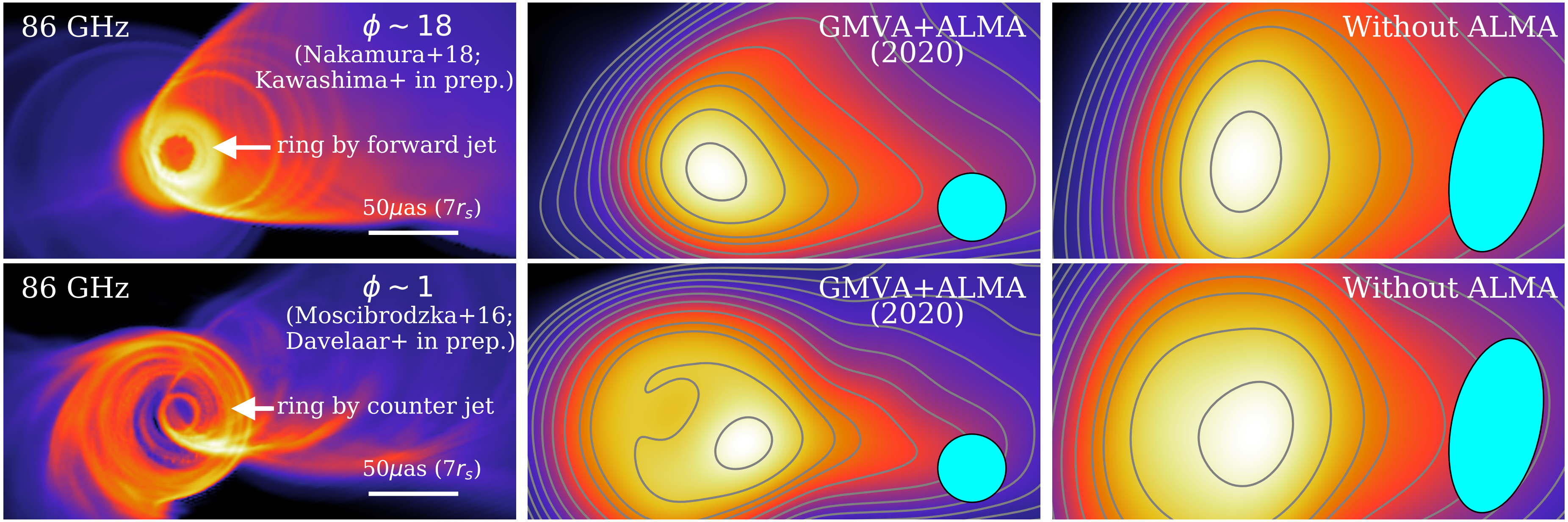

- EHT Collaboration, ALMA Cycle 7 + GMVA Proposal
- GMVA = Europe telescopes + VLBA & more [at 86 GHz]
- Bright counter-jet emission & asymmetric limb-brightening in the small ϕ model

偏光＋ダークマター＋惑星形成の学際的研究

藤田 智弘
（京都大）

田崎 亮
（東北大）

成子 篤
（東北大→京都大）

ガンマ線バースト偏光

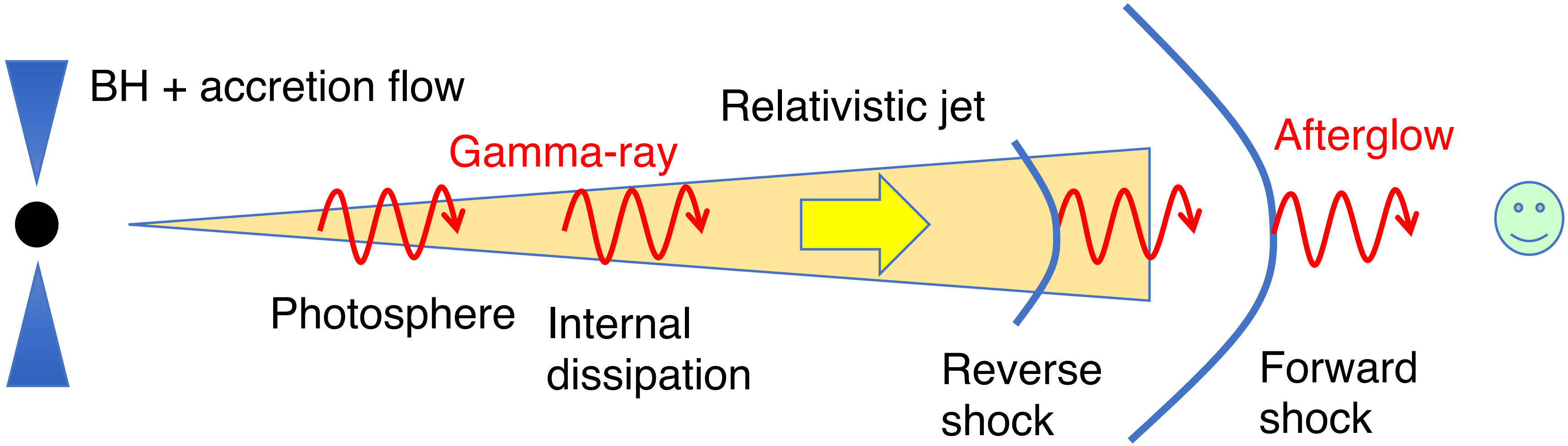

Prompt emission (~100 keV)
GAP, INTEGRAL
(Yonetoku+11;12; Gotz+09;13)
Prompt Opt? (Troja+17)

Late-time Opt afterglow
$\Pi_L \sim$ 1-3% (Covino+03)
$\Pi_C \sim$ 0.6 % (Wiersema+14)
Radio: ALMA?

Early-time Opt afterglow: Liverpool, Kanata
$\Pi_L \sim$ 30% (Mundell+13), $\Pi_L \sim$ 10% (Steele+09),
$\Pi_L \sim$ 10% (Uehara, KT, Kawabata+12)
$\Pi_L <$ 8% (Mundell+07)

ガンマ線バースト偏光と*CPT*対称性

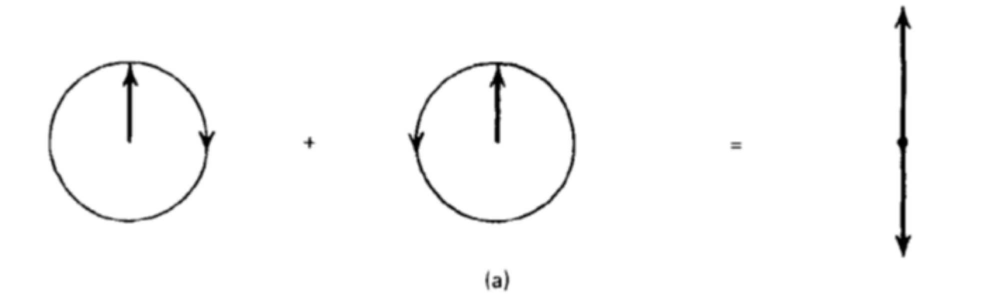

Figure 8.1a ***Decomposition of linear polarization into components of right and left circular polarization.***

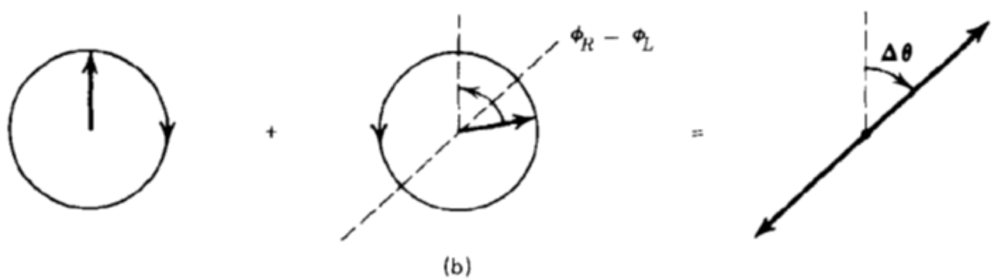

Figure 8.1b ***Faraday rotation of the plane of polarization.***

- ある種の量子重力理論における光の分散関係

$$\omega_\pm \simeq k \pm \frac{\xi}{M_{\rm pl}} k^2$$

- 直線偏光面の回転
- 回転角はエネルギー依存

  広いエネルギーバンドの積分で消偏光

- Π(70-300keV) > 35% (2σ) for GRB110721A (D > 2.5Gpc)

➡ $|\xi| < 2 \times 10^{-15}$,

KT, Mukohyama, Yonetoku et al. 2012;
Myers & Pospelov 2003

アクシオンダークマター

$$\omega_{\pm} \simeq k \pm \frac{-1}{2} g_{a\gamma} \dot{\phi}$$

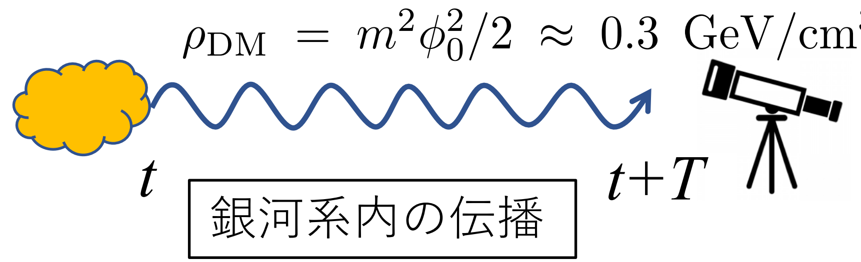

- 回転角は光子振動数に依存しない
  - 天体の偏光面を知っていなければこの効果を調べられない

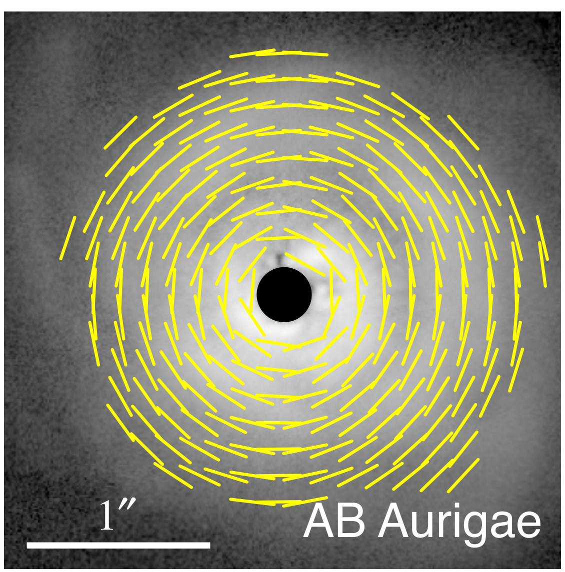

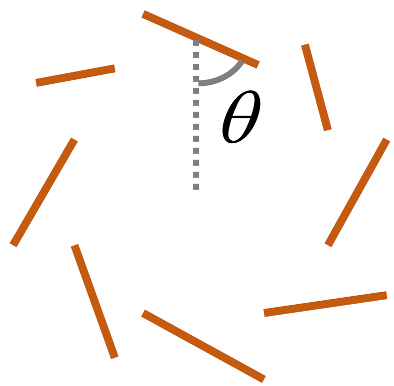

Axion effect?

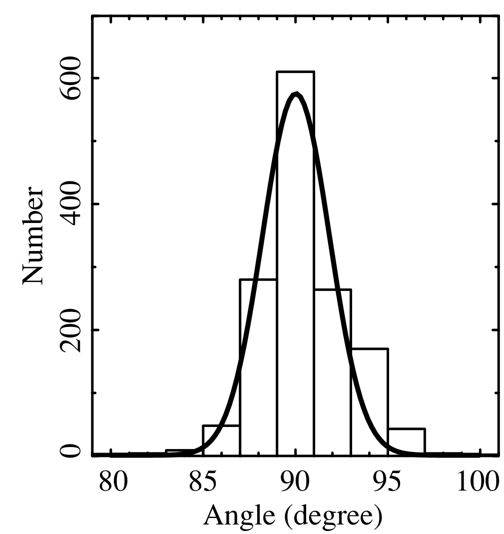

$g_{a\gamma}$への制限

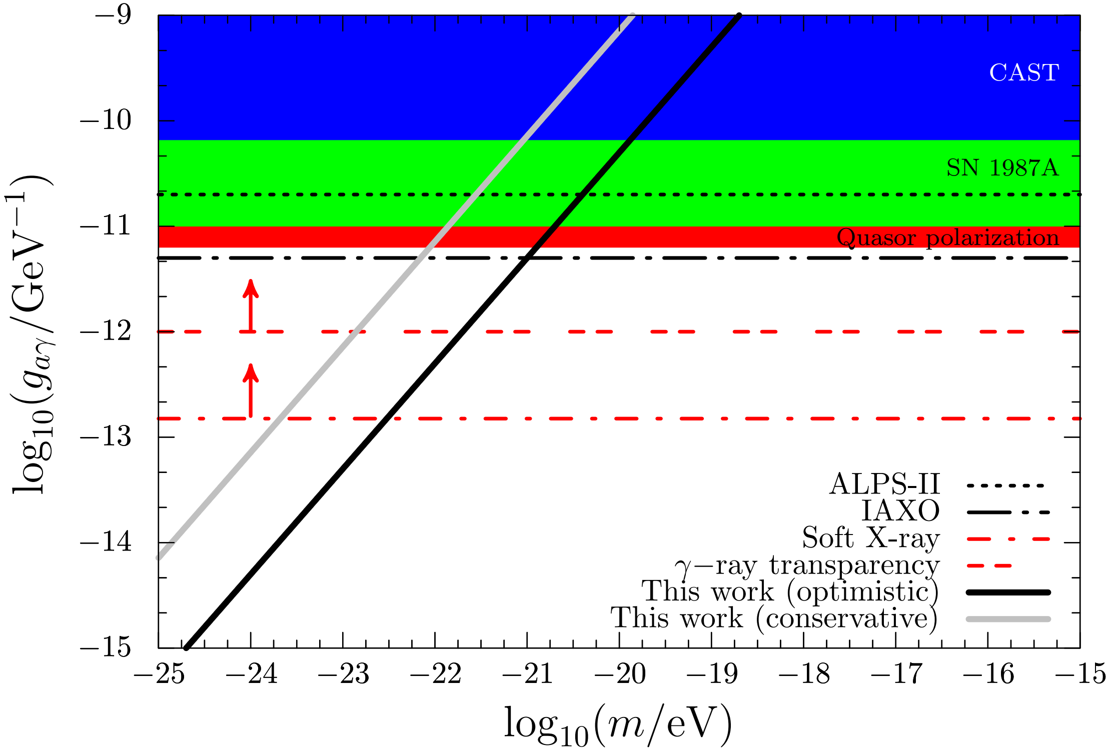

- $m < 10^{-21}$ eVの結合定数にこれまでで最も厳しい上限を与える
- 予言：偏光角の時間変動 $t_{\rm p} \sim \frac{\hbar}{mc^2} \sim 1.3/(m/10^{-22}\ \mathrm{eV})\ \mathrm{yr}$

Fujita, Tazaki & KT 2019

Summary

- BHジェット：相対論とプラズマ物理が関わる問題
  - 駆動、加速、絞り込み、安定性、散逸、粒子加速
- 観測の発展が著しく、様々な分野と関連
  - 超高解像度電波観測、偏光、マルチメッセンジャー、時間軸天文学
- Event Horizon Telescopeの初期成果
  - 一般相対論の検証、銀河中心BHが存在することが確定
  - 偏光解析
  - 望遠鏡の数を増加, 345GHz観測
- BZ processをいかに観測的に証明するか

- 偏光・ダークマター・惑星形成の学際研究
- 一つのテーマに注力し、しかしそれに止まらない姿勢が大切

パルサー風

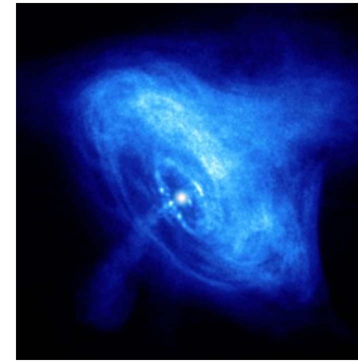

(Goldreich & Julian 1969)

$$\mathbf{S}_{\rm p} = \frac{\mathbf{E}\times\mathbf{B}_\varphi}{4\pi}$$

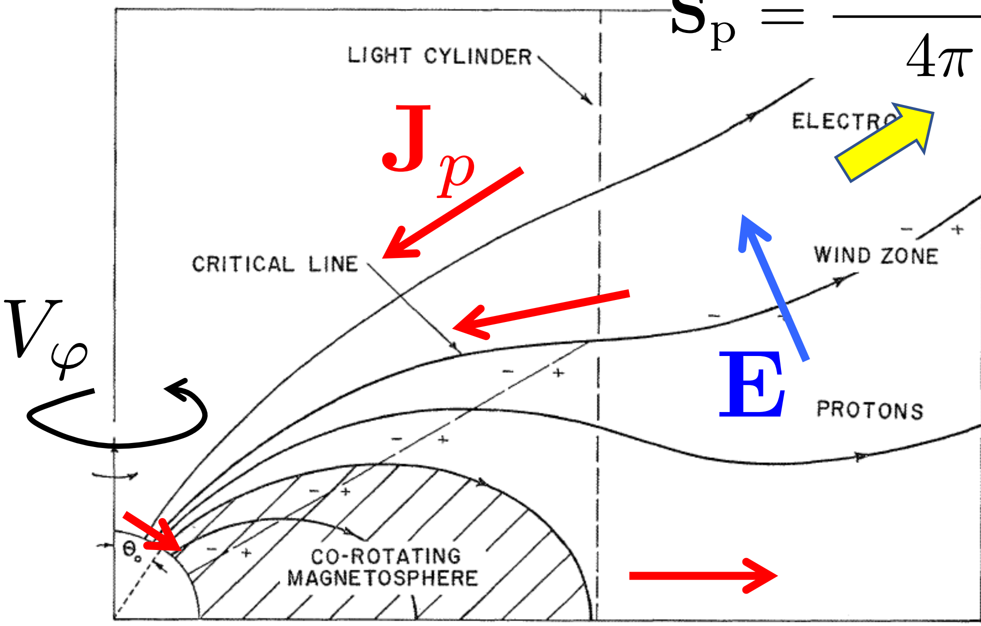

$$\mathbf{E} = -\mathbf{V}_\varphi \times \mathbf{B}$$

$$\nabla\cdot\mathbf{S}_{\rm p} = -\mathbf{E}\cdot\mathbf{J}_{\rm p} > 0$$

Steady, axisymmetric

$$\nabla\times\mathbf{E} = 0 \;\Rightarrow\; \mathbf{E} = -\nabla\phi$$

$$\Rightarrow\; E_\varphi = 0$$

Electric field screened by plasma

$$\mathbf{E}\cdot\mathbf{B} = 0$$

$$\Rightarrow\; \mathbf{E} = -\frac{r\Omega_{\rm F}}{c}\mathbf{e}_\varphi \times \mathbf{B}$$

$$\Omega_{\rm F} = \Omega_{\rm pulsar}$$

BHs with largest angular sizes

Object	M_{BH} ($10^8 M_{sun}$)	d (Mpc)	1Rs (μas)
SgrA*	0.04	0.008	10
M87	60 (30?) Stellar dynamics (gas dynamics)	16.7	7
Sombrero	10	9.0	2.2
M84	8.5	17	1
Cen A	0.5	3.8	0.3

$(= 2r_g = 2GM/c^2)$

Location of the engine

VLBA 7mm

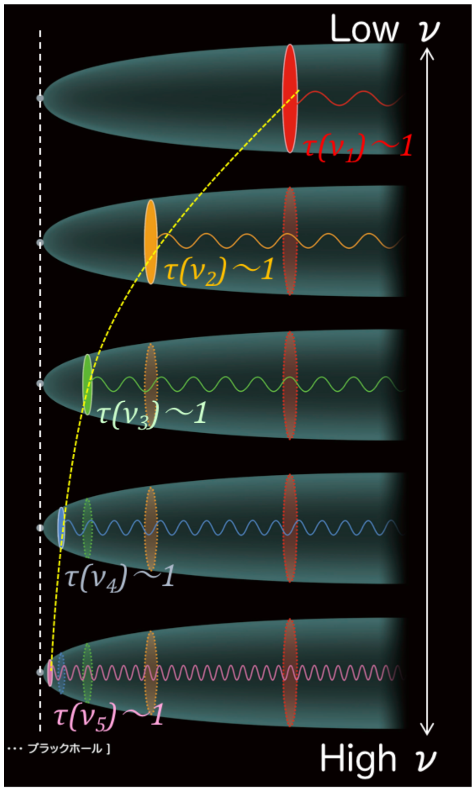

Core-shift
(Blandford & Konigl 1979)

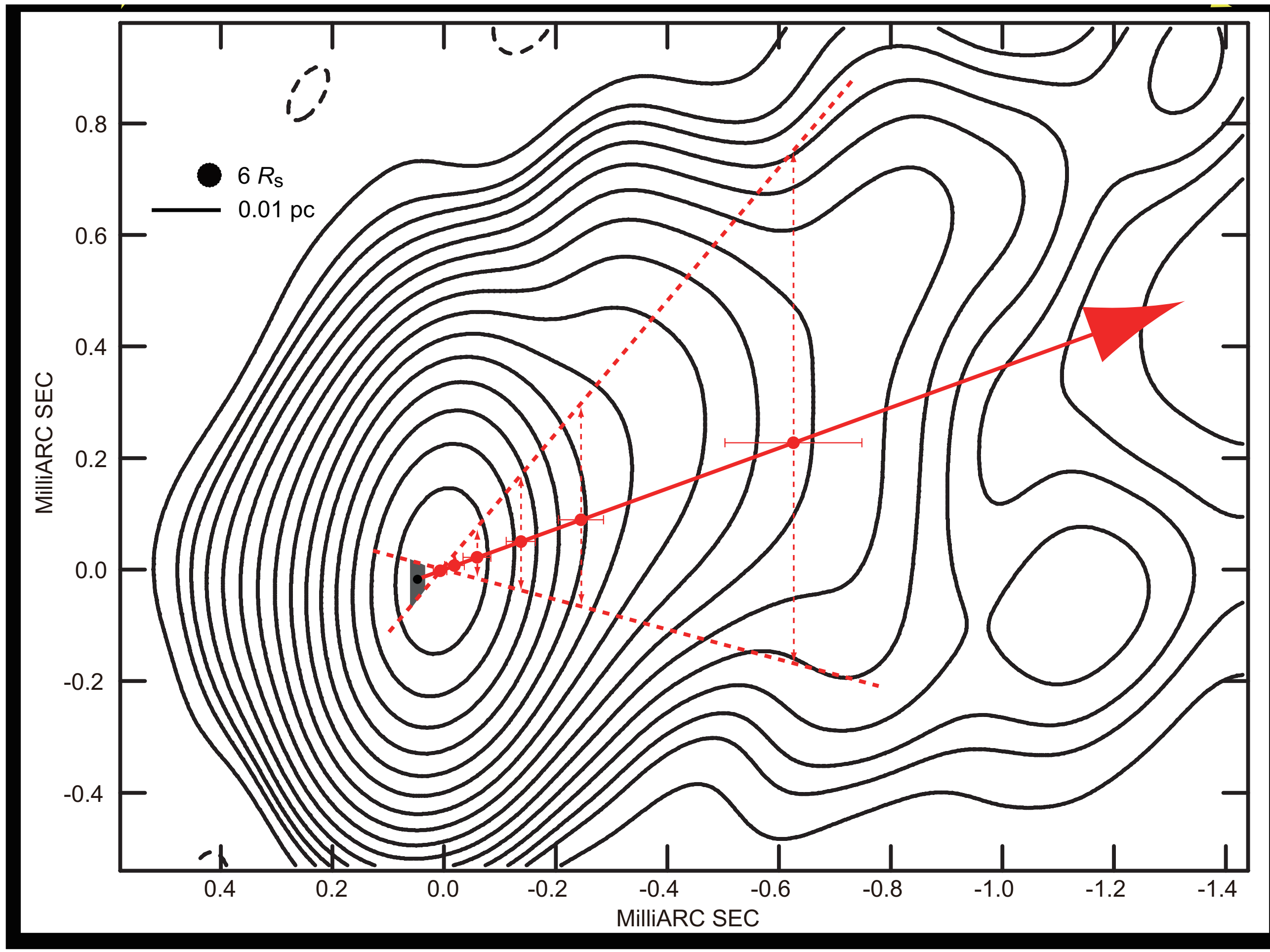

- High-accuracy core-shift measurement suggests the central engine resides very close to 7mm core

Hada+2011

Image models

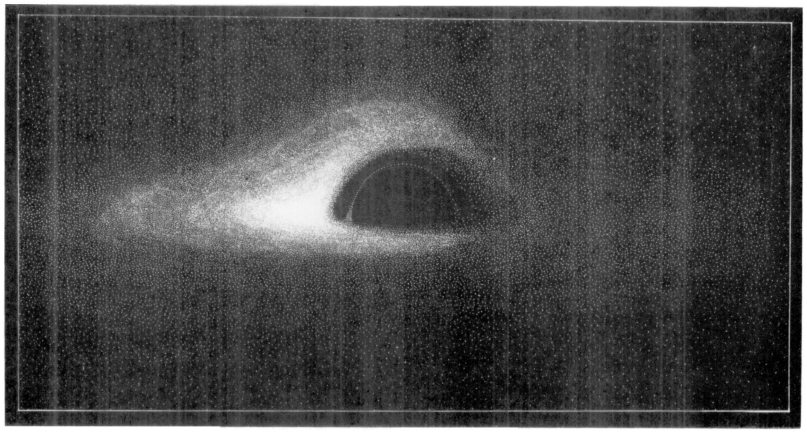

Fig. 11. Simulated photograph of a spherical black hole with thin accretion disk

- Standard disk model

Luminet 1979; Bardeen 1973

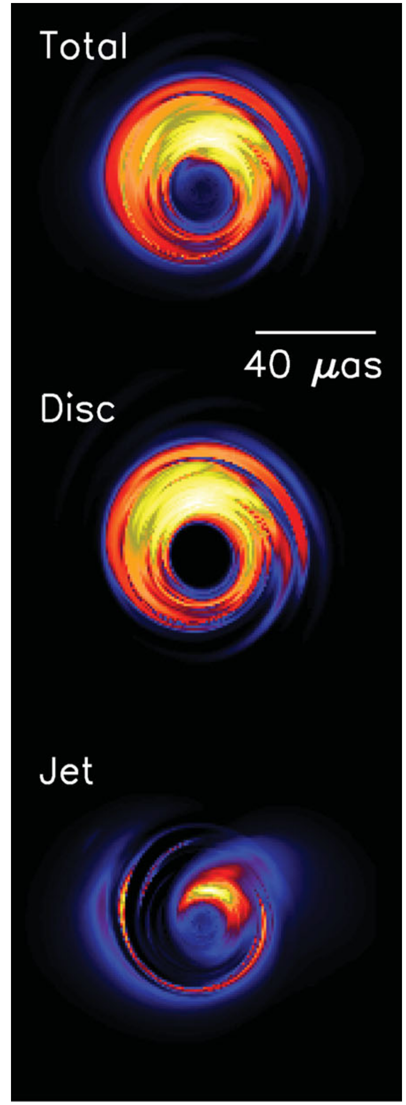

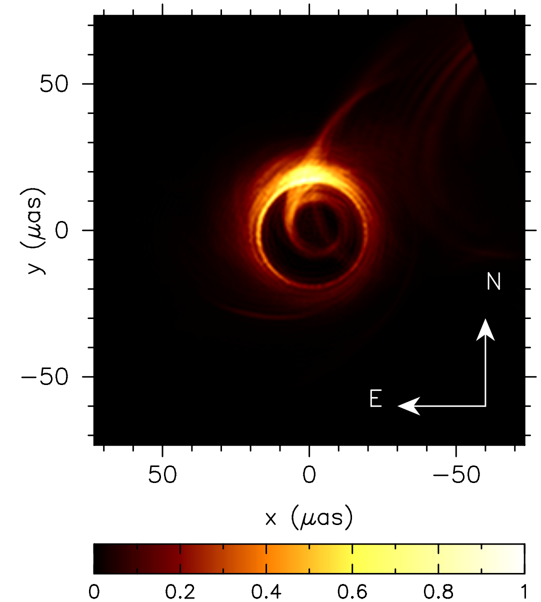

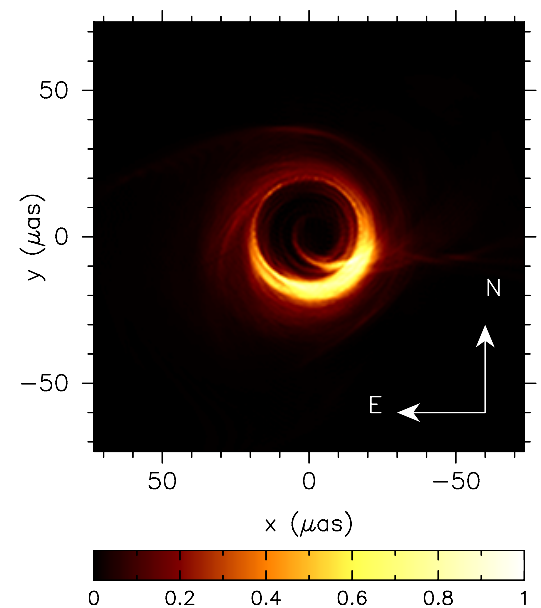

- RIAF + jet models (GRMHD simulations + GRRT calculations)

Falke, Melia & Agol 2000; Dexter+2012; Moscibrozka+2016

Photon ring

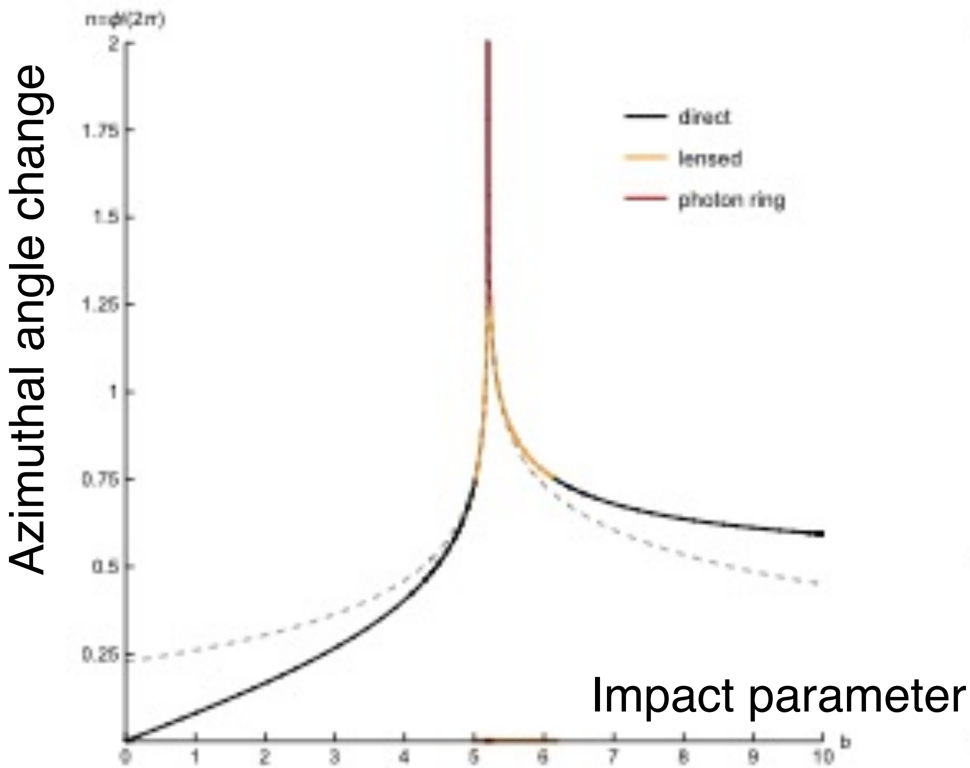

Schwarzschild BH

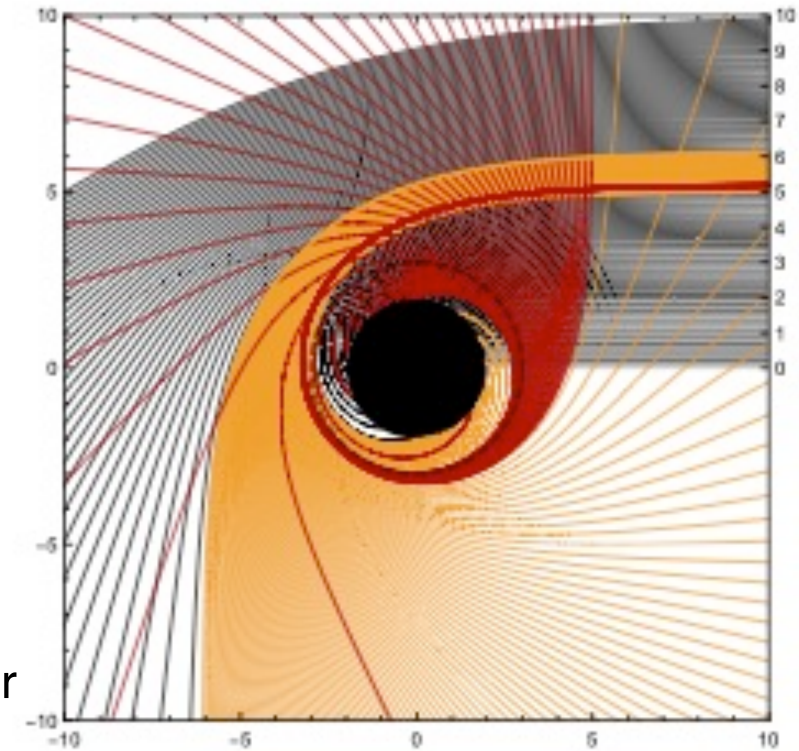

- Photons which are seen near the critical curve will have orbited the BH many times and then pick up extra brightness on their way to the observer
- Photon ring (+ lensing ring) is bright in the optically-thin case

Gralla, Holz & Wald 2019

Rough estimates

$$T_i \sim 0.3\, T_{i,\mathrm{vir}} \simeq 10^{12} \left(\frac{r_g}{r}\right) \ \mathrm{K}$$

$$\begin{cases} n_i k_\mathrm{B} T_i + n_e k_\mathrm{B} T_e = \beta_\mathrm{p} B^2 / 8\pi \\ F_\nu = \dfrac{4\pi r^3 n_e}{3D^2} \left[\sqrt{2}\pi \dfrac{e^2 \nu_\mathrm{s}}{6\pi \Theta_e^2 c} \left(\dfrac{\nu}{\nu_\mathrm{s}}\right) e^{-\left(\frac{\nu}{\nu_\mathrm{s}}\right)^{\frac{1}{3}}}\right] \end{cases}$$

~ 0.5 Jy

Optically-thin thermal e synchrotron (Leung+2011)

$$\nu_\mathrm{s} = \frac{eB}{9\pi m_e c} \Theta_e^2 \sim 0.3 \left(\frac{\Theta_e}{10}\right)^2 \ \mathrm{GHz}$$

$$n_e \simeq 3 \times 10^4 \left(\frac{r}{r_g}\right)^{-1.3} \beta_\mathrm{p}^{0.62} \left(\frac{T_i}{3T_e}\right)^{-0.47} \left(\frac{T_e}{10T_b}\right)^{-2.4} \mathrm{cm}^{-3}$$

$$B \simeq 5 \left(\frac{r}{r_g}\right)^{-0.63} \beta_\mathrm{p}^{-0.19} \left(\frac{T_i}{3T_e}\right)^{0.14} \left(\frac{T_e}{10T_b}\right)^{-0.71} \mathrm{G}$$

$T_\mathrm{b} \sim 6 \times 10^9$ K

GRMHD simulation library

- Kerr BH with fixed M & a_*
- 3D ideal MHD models
- Codes: BHAC (Porth+17), H-AMR (Liska+18), iharm (Gammie+03), KORAL (Sadowski+13)

- Initial condition: hydrodynamically static torus + poloidal B field
  - Accretion flow AM II BH spin
- Outflow-only boundary condition
- Density floor

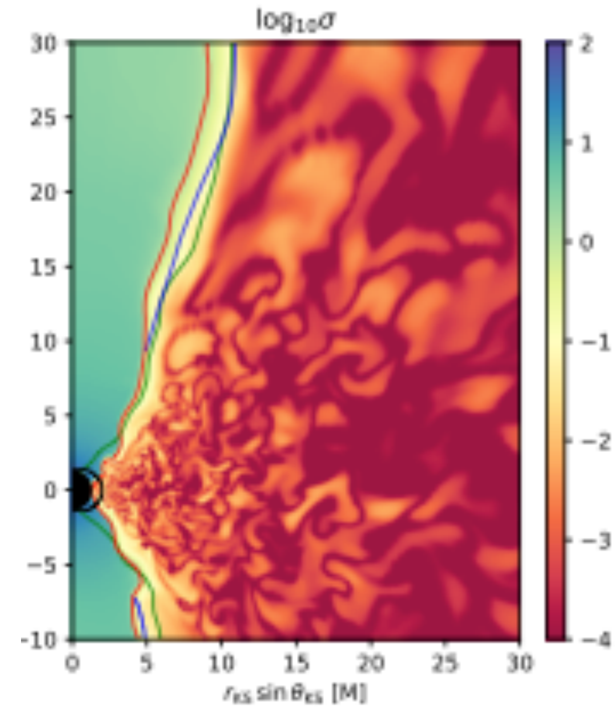

Porth+ 2019

- Quasi-steady state at $r <\sim 10\ r_g$: $5000 <\sim t/r_g\ c^{-1} <\sim 10^4$
- 2 key parameters: normalized magnetic flux & BH spin
  - SANE models ($\phi \sim 3$): $a_* = -0.94, -0.5, 0, 0.5, 0.75, 0.88, 0.94, 0.97, 0.98$
  - MAD models ($\phi > 50$): $a_* = -0.94, -0.5, 0, 0.5, 0.75, 0.94$

$$\phi \equiv \Phi_{BH}(\dot{M} r_g^2\ c)^{-1/2}$$

GR Ray-Tracing calculations

- Thermal electrons assumed, with one parameter $R_{\rm high}$
  (cf. Howes 2006; Kawazura+2018)

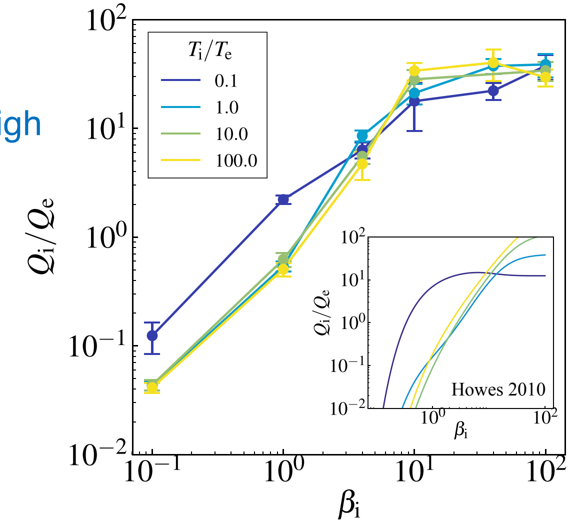

$$R \equiv \frac{T_i}{T_e} = R_{\rm high}\frac{\beta_{\rm p}^2}{1+\beta_{\rm p}^2} + \frac{1}{1+\beta_{\rm p}^2}$$

- Emission from regions with $B^2 > \rho c^2$ (i.e. funnel region) is set to zero
- 100-500 images from each GRMHD models,
  each of $R_{\rm high}$ = 1, 10, 20, 40, 80, 160
  inclination i = 12°, 17°, 22°, 158°, 163°, 168° (not highly affect image)
- Various codes that include RAIKOU (Kawashima+)

- MHD velocity field is invariant under scaling ρ -> $C\rho$, B -> $C^{1/2}B$, u -> Cu
- C is adjusted for F_ν ~ 0.5 Jy, then M determines ring size & $\dot{M} \sim 4\pi r^2 \rho v^r$

Photon orbits

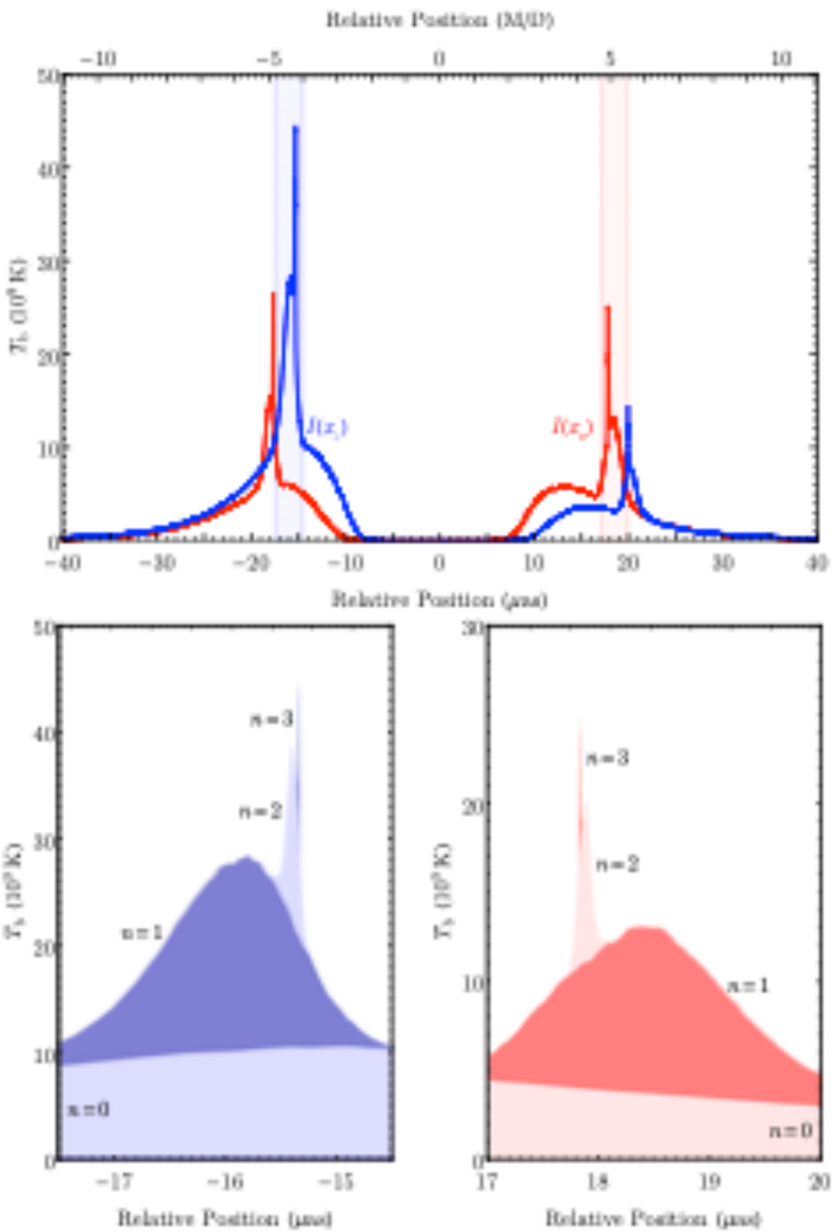

Johnson+2019

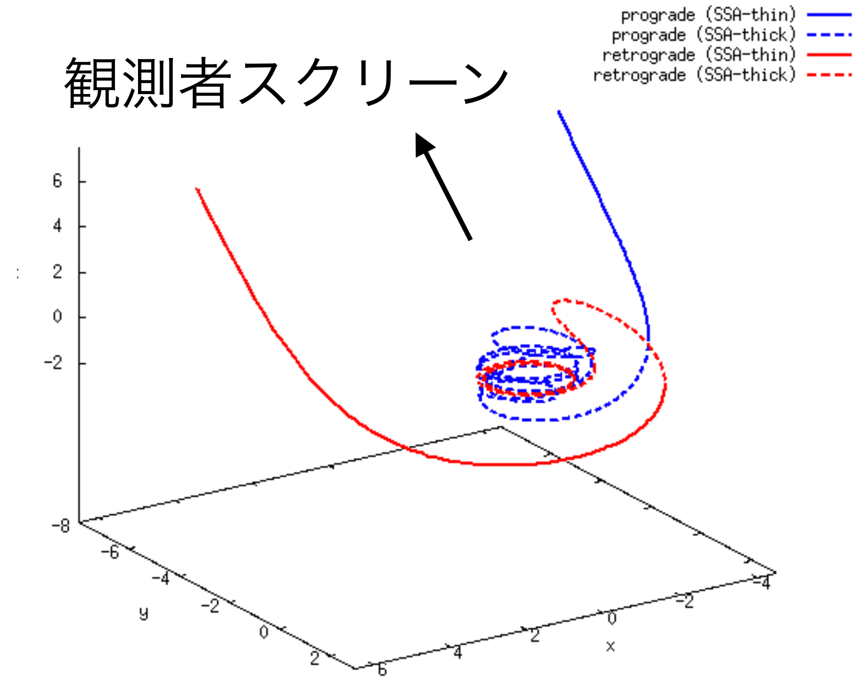

Credit: Kawashima (cf. Kawashima+2019)

- Time-averaged images
- i = 163 deg (Accretion disk angular momentum)
- Arrows: BH spin vector projected onto the sky
- Asymmetry is controlled by the BH spin (except the SANE $R_{\rm high} < 10$)
- Much emission comes from the funnel wall that rotates in a similar way as the BH
- Doppler beaming

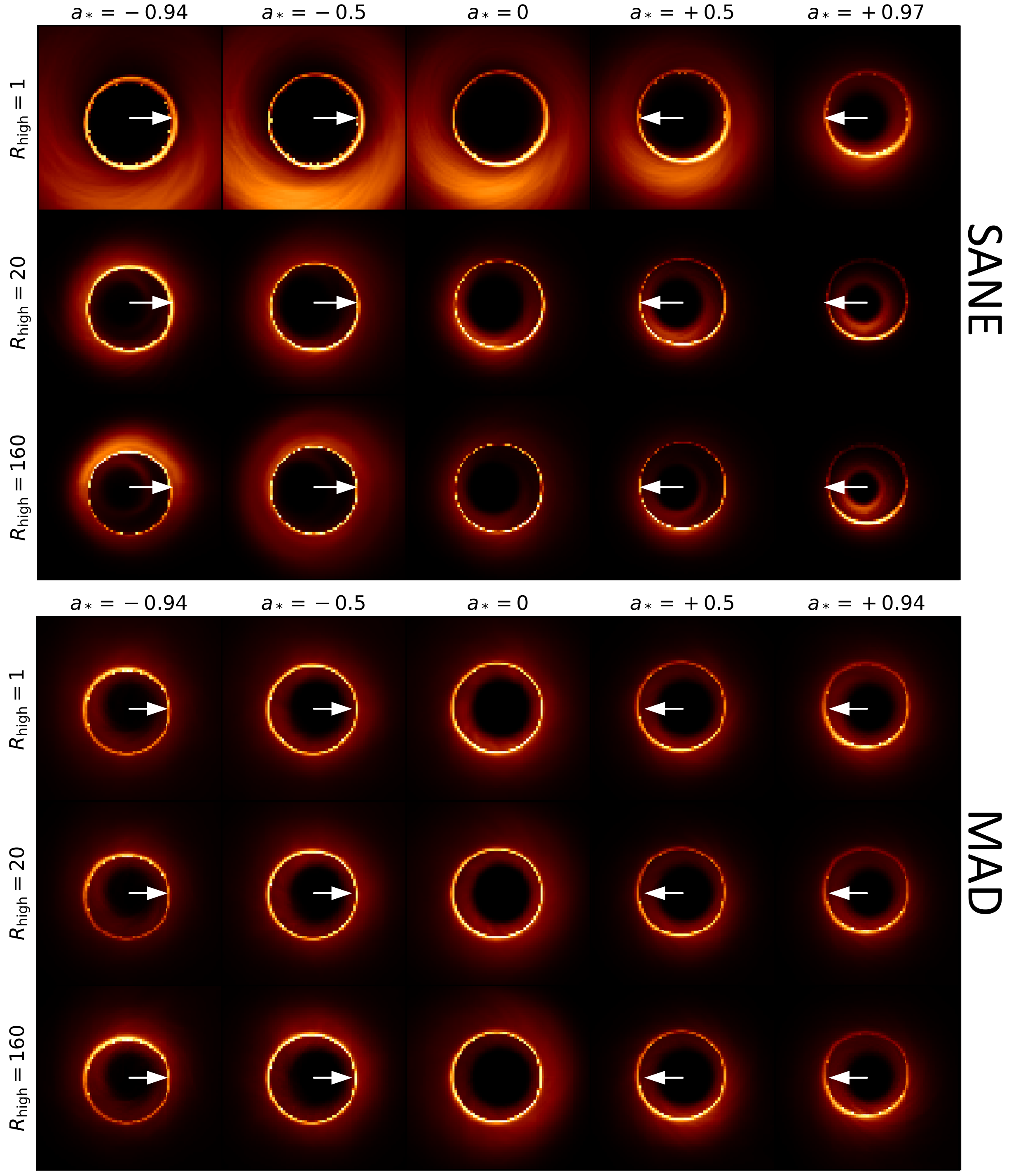

- Prograde models: $a_* > 0$
- Location of the origin for all photons that make up an image
- Emission at $1 < r/r_g < 4$ (unstable photon orbit region) dominant
- The funnel wall is bright for high R_{high} cases

- Funnel is wider for MAD than for SANE

$a_* = +0.94$

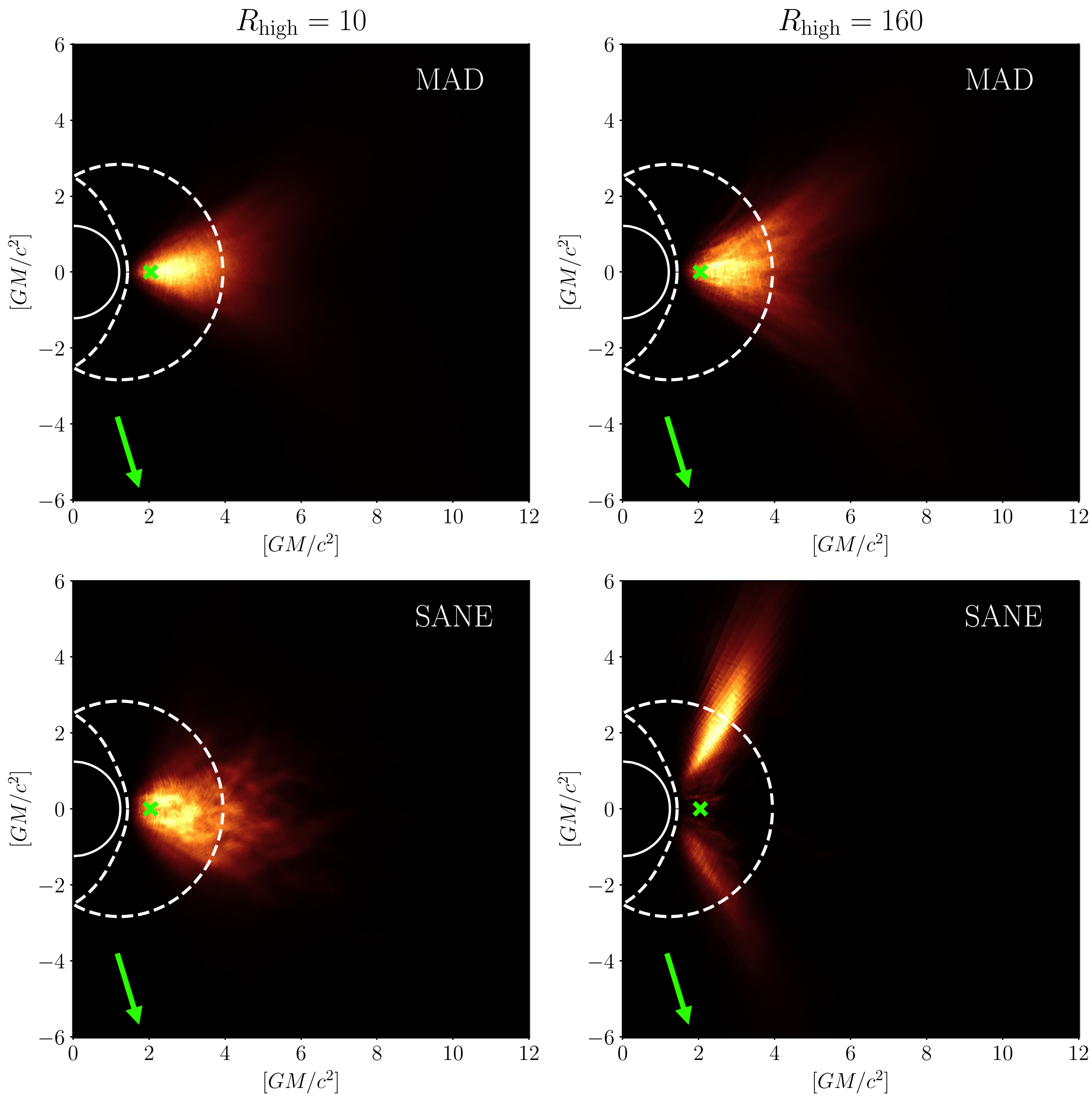

- Retrograde models: $a_* < 0$
- ISCO radius is much larger
- MAD funnel widths are similar in pro- and retro-grade cases (cf. Tchekhovskoy & McKinney 2012)
- Even in SANE models, funnel is wide

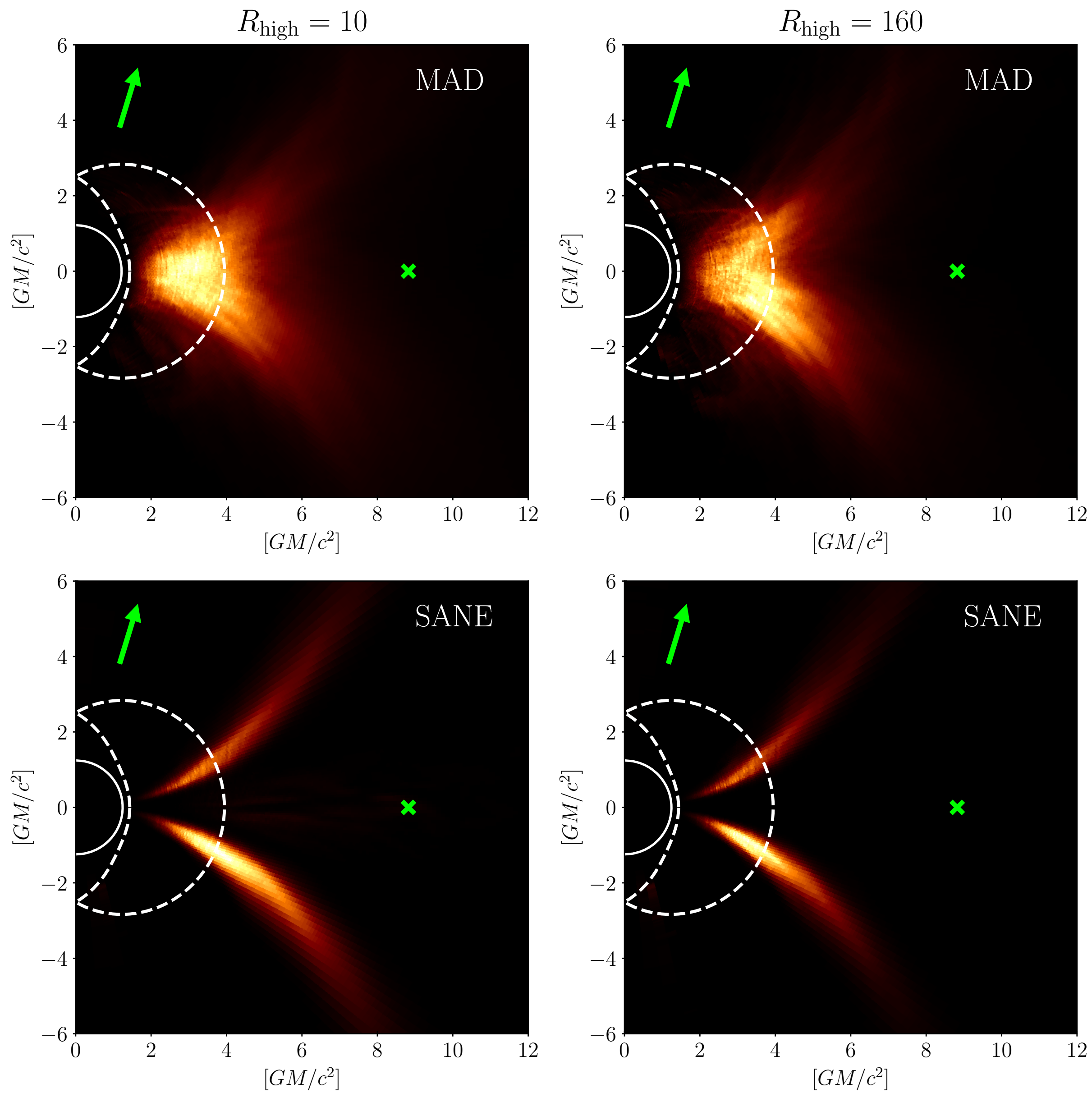

Model fitting

- Probability distribution of parameters *M/D*, *C*, and PA via MCMC method
- Each simulation code derive similar distribution

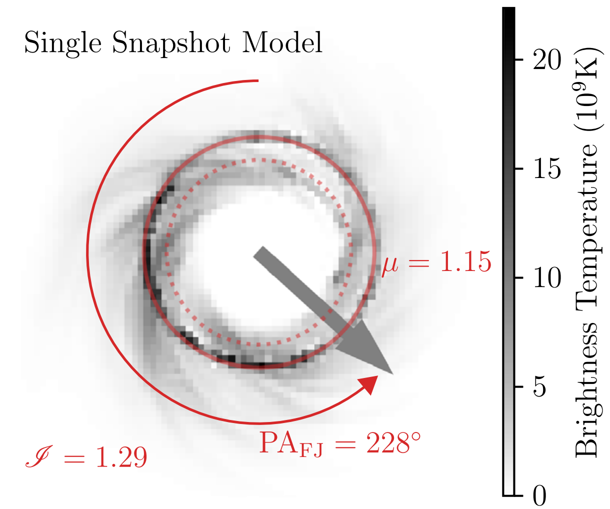

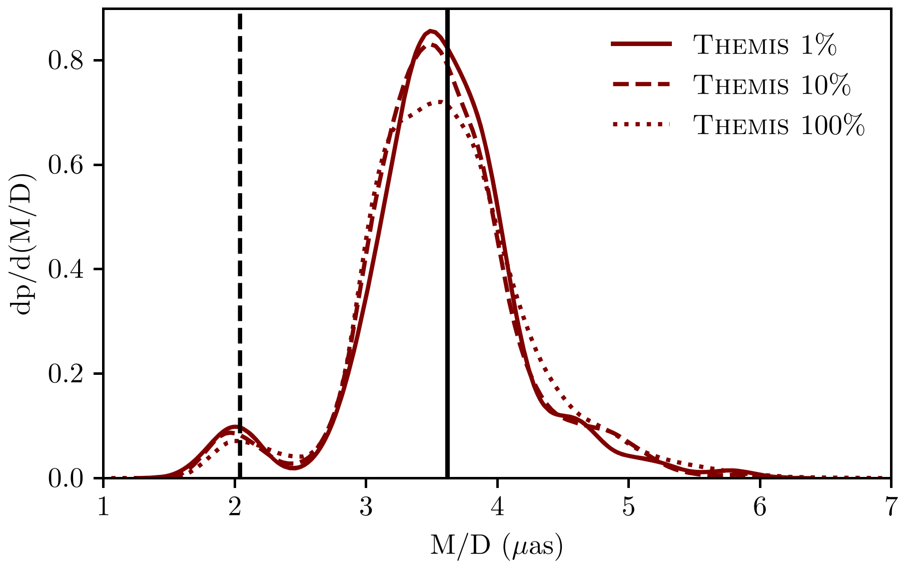

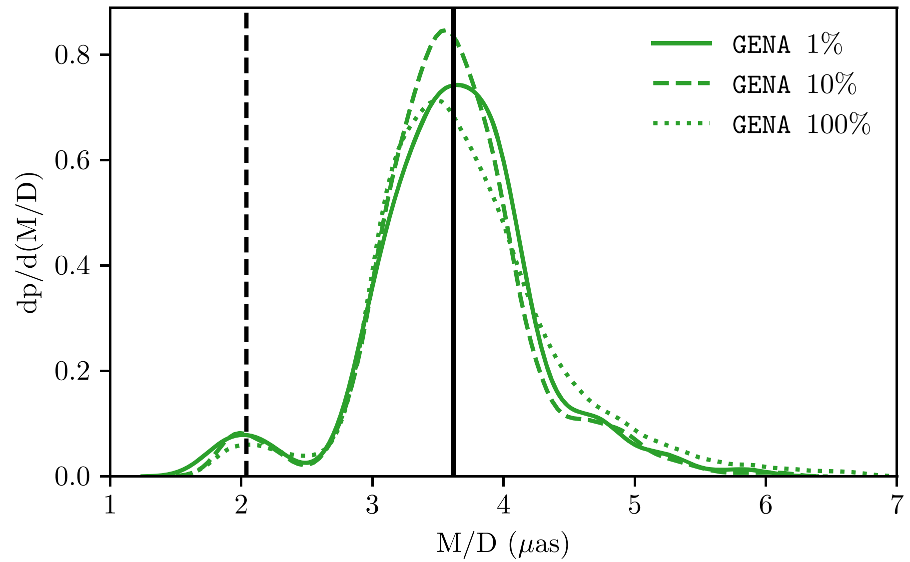

- $M \sim 6.5^{+0.7}_{-0.6}$ x10^9 M_{sun} (derived in paper VI)
- Consistent with the previous estimates based on stellar dynamics

PA ~ 288°, large-scale jet orientation

$i < 90°$, $a_* < 0$
$i > 90°$, $a_* > 0$

These cases are more likely

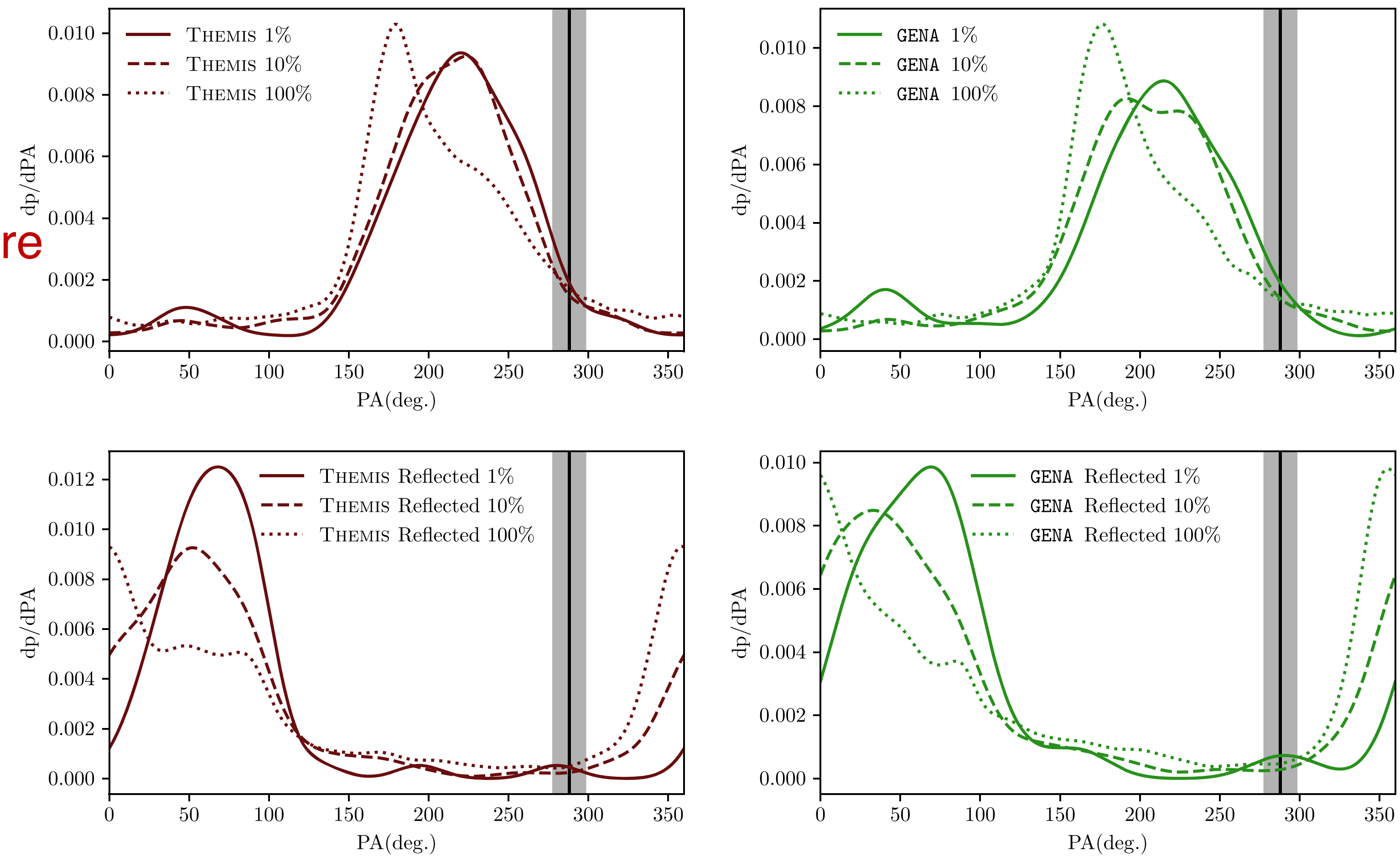

$i < 90°$, $a_* > 0$
$i > 90°$, $a_* < 0$

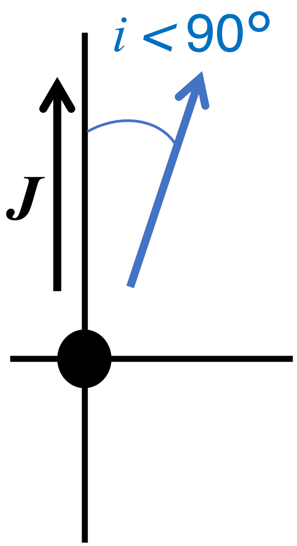

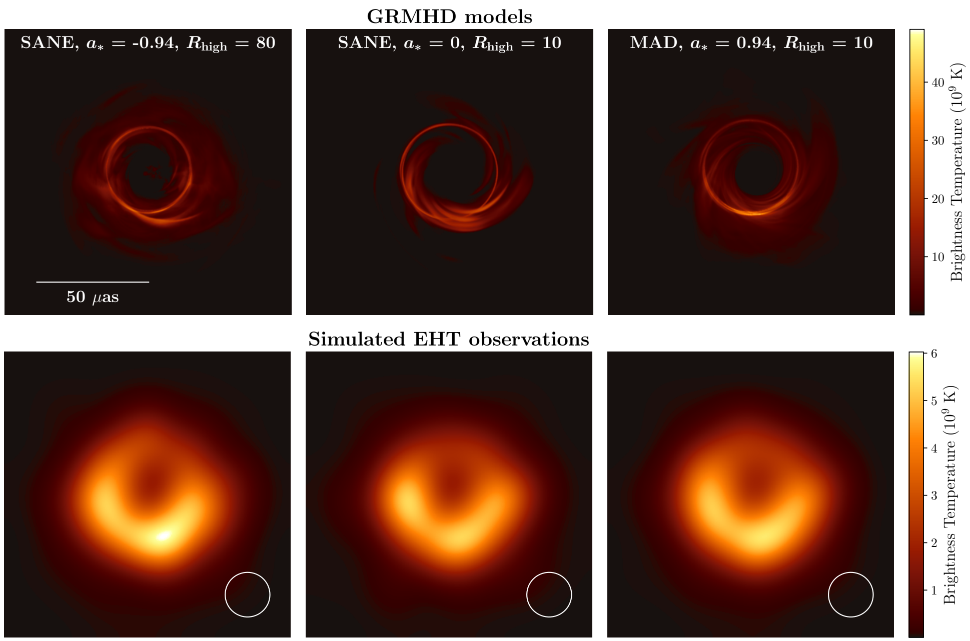

Average Image Scoring[a] Summary

Flux[b]	a_*[c]	$\langle p \rangle$[d]	N_{model}[e]	MIN(p)[f]	MAX(p)[g]
SANE	−0.94	0.33	24	0.01	0.88
SANE	−0.5	0.19	24	0.01	0.73
SANE	0	0.23	24	0.01	0.92
SANE	0.5	0.51	30	0.02	0.97
SANE	0.75	0.74	6	0.48	0.98
SANE	0.88	0.65	6	0.26	0.94
SANE	0.94	0.49	24	0.01	0.92
SANE	0.97	0.12	6	0.06	0.40
MAD	−0.94	0.01	18	0.01	0.04
MAD	−0.5	0.75	18	0.34	0.98
MAD	0	0.22	18	0.01	0.62
MAD	0.5	0.17	18	0.02	0.54
MAD	0.75	0.28	18	0.01	0.72
MAD	0.94	0.21	18	0.02	0.50

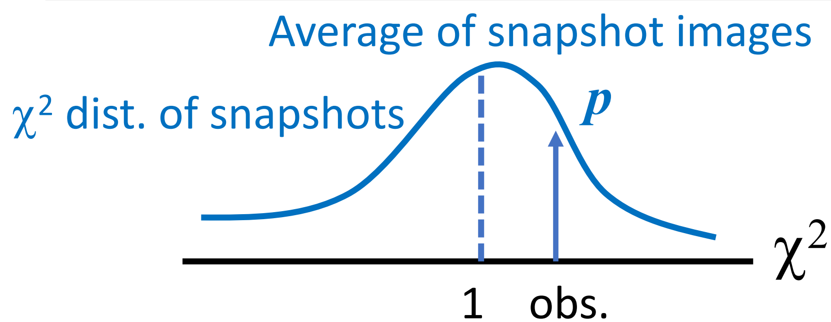

- Overall, the observed image is consistent with expectations for the shadow of a Kerr BHs predicted by general relativity
- So many models are acceptable. This is likely because the source structure is dominated by the photon ring
- If the BH spin and M87's large scale jet are aligned, then the BH spine vector is pointed away from Earth

Other constraints

- Radiative efficiency
  - $L_{\rm bol}$/Mdot c^2 < thin disk radiative efficiency

- Simultaneous X-ray observation (2-10 keV)
  - Single IC scattering of synchrotron photons

- $P_{\rm jet} \sim 10^{42} - 10^{45}$ erg/s
  - Conservative lower limit: 10^{42} erg/s
  - All a_*=0 models rejected
  - SANE models with $|a_*|$=0.5 rejected

$$P_{\rm BZ} \approx 2.8 f(a_*)(\phi/50)^2 \dot{M} c^2 \qquad f(a_*) \approx a_*^2 (1 + \sqrt{1 - a_*^2})^{-2}$$

(for $a_* < 0.95$)

Other constraints

- SANE models: EHT image, radiative efficiency, X-ray, jet power

a/R_{high}	1	10	20	40	80	160
-0.94	-+++	++++	++++	++++	++++	-+++
-0.5	++- -	++- -	+++-	+++-	-++-	++-+
0	+++-	+++-	++- -	+++-	++- -	++- -
0.5	+++-	+++-	+++-	+++-	+++-	+++-
0.94	+-+-	+-+-	+++-	+++-	++++	++++

$Mdot/Mdot_{Edd} \sim 10^{-5} – 10^{-4}$

Other constraints

- MAD models: EHT image, radiative efficiency, X-ray, jet power

a/R_{high}	1	10	20	40	80	160
-0.94	- -++	-+++	-+++	-+++	-+++	-+++
-0.5	+-+-	+++-	++++	++++	++++	++++
0	+-+-	+++-	+++-	+++-	+++-	+++-
0.5	+-+-	++++	++++	++++	++++	++++
0.94	+- -+	+-++	++++	++++	++++	++++

$Mdot/Mdot_{Edd} \sim 10^{-6}$

Discussion

- Radiative effects: GRMHD vs radiation GRMHD
- Non-thermal electrons
- Analysis limitations
  - Fast light approximation
  - Untilted disks
  - Pair production
  - Floors

- Alternatives to Kerr BHs

EHT data + EAVN data

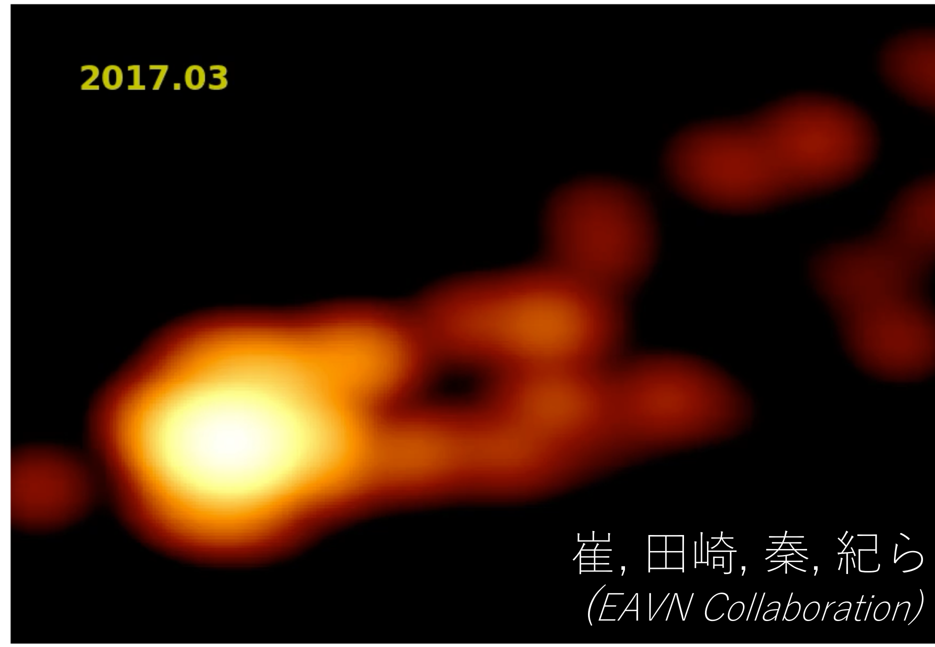

- High cadence observations of M87/SgrA*
- Data quality comparable to VLBA
- 22/43 GHz → spectral index

EHT 2020 forecast

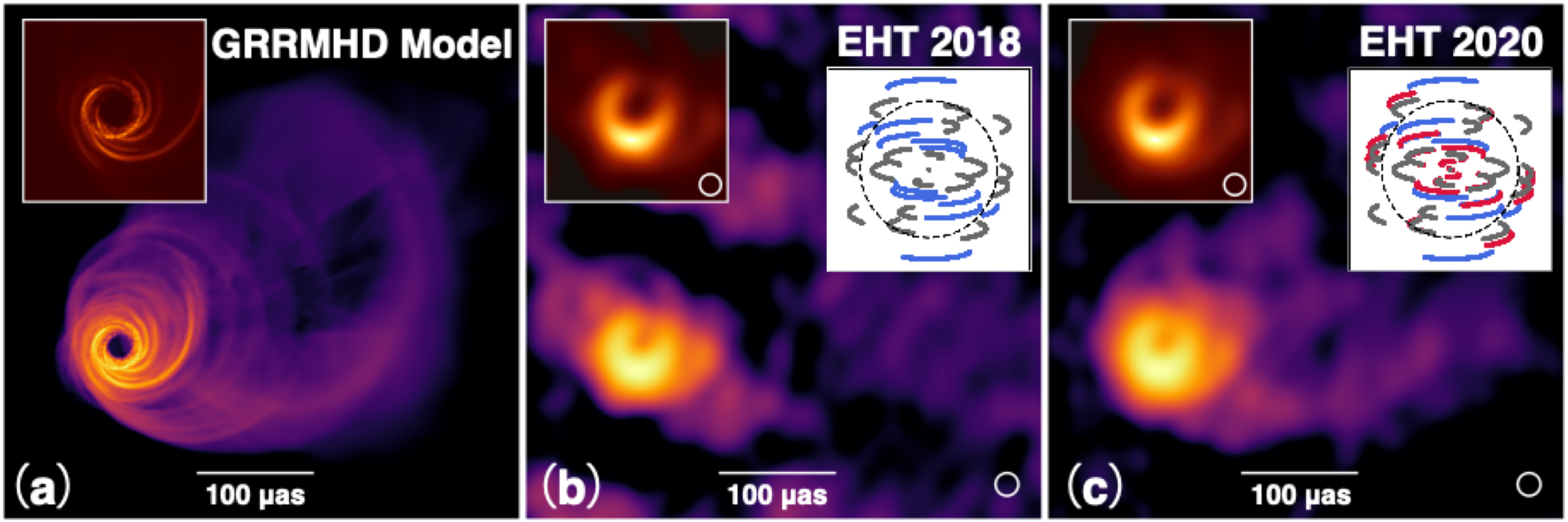

- EHT Collaboration, ALMA Cycle 7 M87 Proposal
- 3 more telescopes including Green Land Telescope will make it so sensitive as to detect extended component

Event Horizon Telescope

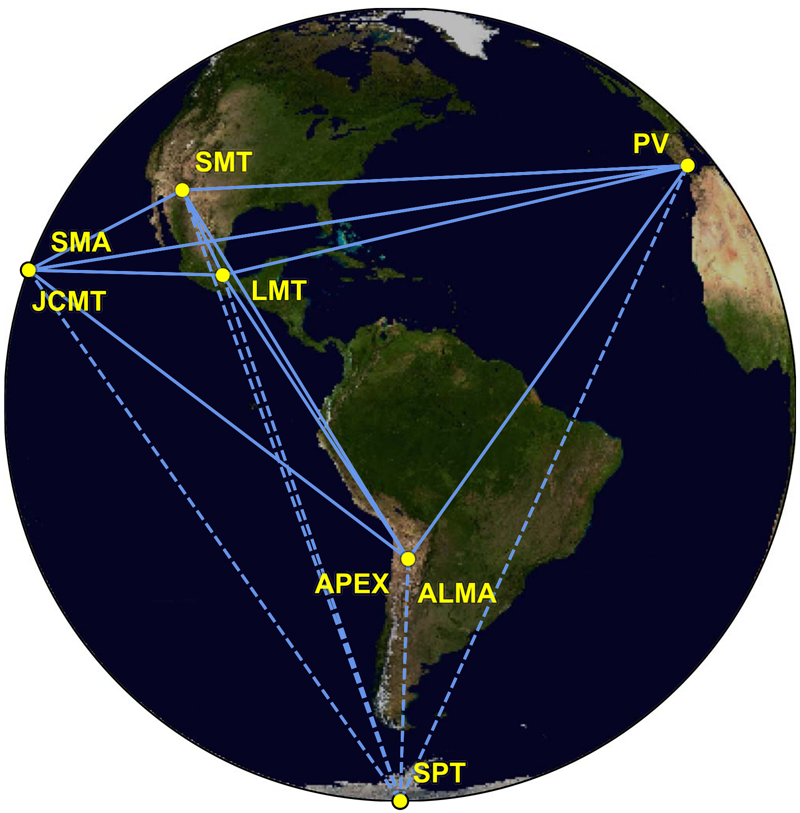

Figure 1. Eight stations of the EHT 2017 campaign over six geographic locations as viewed from the equatorial plane. Solid baselines represent mutual visibility on M87* (+12° declination). The dashed baselines were used for the calibration source 3C279 (see Papers III and IV).

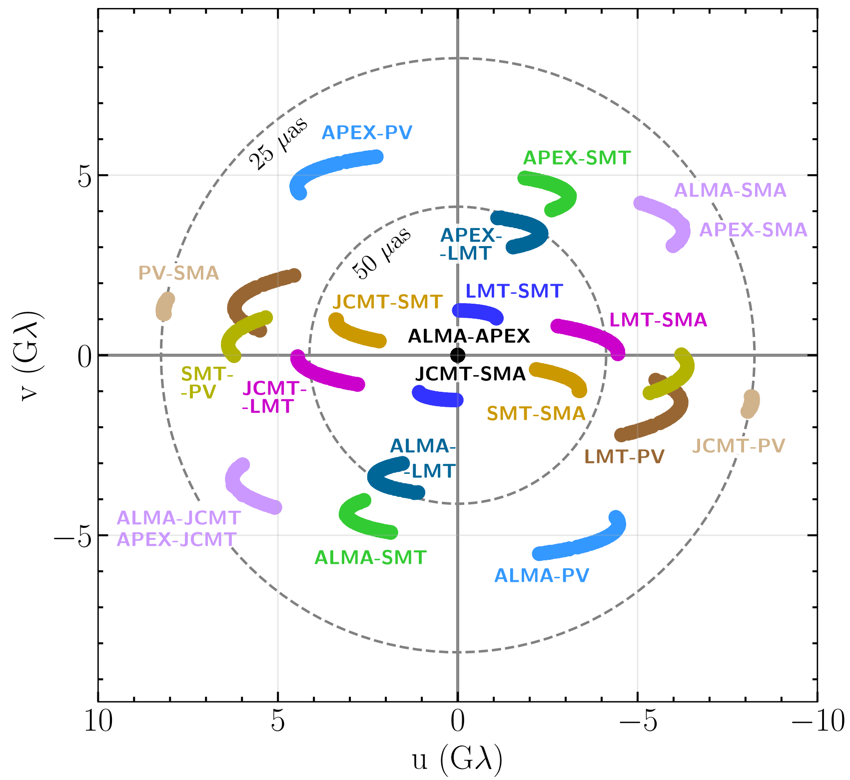

- Angular resolution θ ~ 1.3 mm/10^4 km ~ 25 μas

イベント・ホライズン・テレスコープ（EHT）

― 各地の電波望遠鏡をつなぎ、地球サイズの仮想望遠鏡を構成 ―

2018年の観測

ALMA	アルマ望遠鏡	チリ・アタカマ砂漠
APEX	APEX	チリ・アタカマ砂漠
30-M	IRAM 30m望遠鏡	スペイン・ピコベレタ
JCMT	ジェームズ・クラーク・マクスウェル望遠鏡	ハワイ・マウナケア
LMT	大型ミリ波望遠鏡	メキシコ・シエラネグラ
SMA	サブミリ波干渉計	ハワイ・マウナケア
SMT	サブミリ波望遠鏡	アリゾナ・グラハム山
SPT	南極点望遠鏡	南極点基地
GLT	グリーンランド望遠鏡	デンマーク・グリーンランド チューレ空軍基地

2020年に参加

Kitt Peak	キットピーク12m望遠鏡	アリゾナ・キットピーク
NOEMA	NOEMA観測所	フランス・プラトーデビュール

NSF AUI NRAO

Parametrize electron distribution

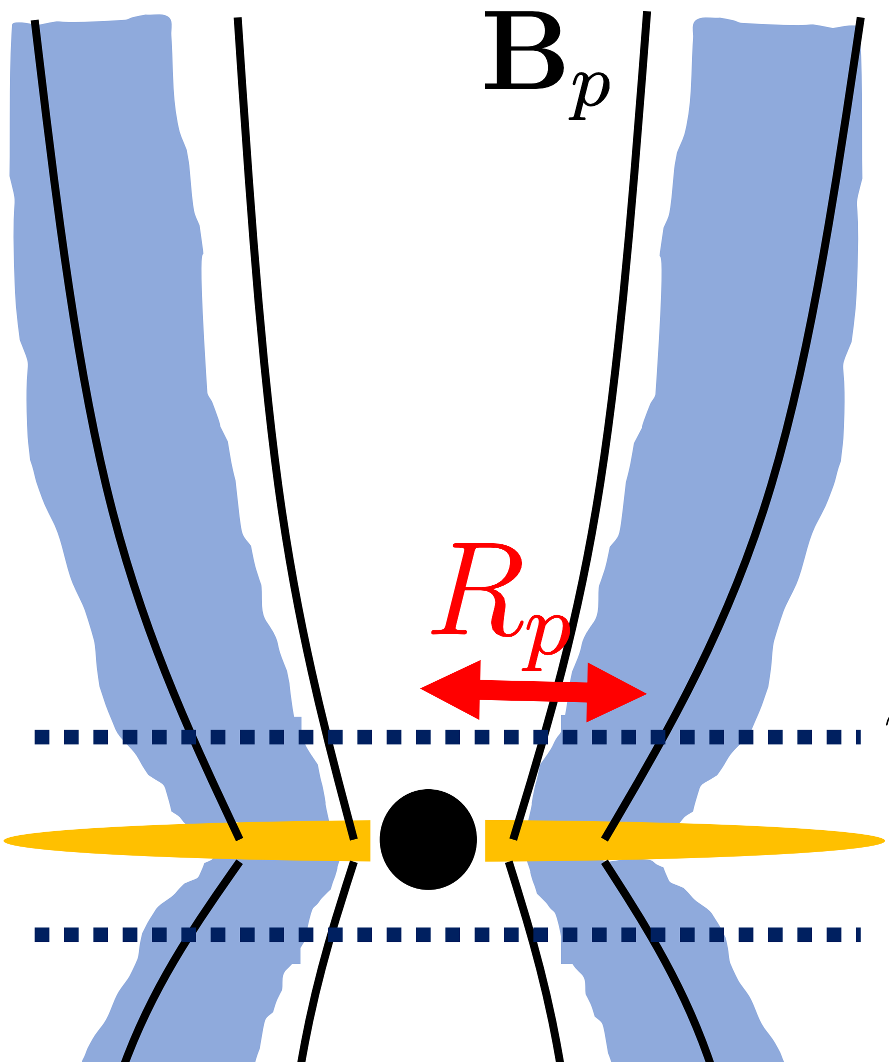

$$\nabla \cdot (n\mathbf{v}) = 0$$

$$\Rightarrow \quad \mathbf{B} \cdot \nabla \left(\frac{n}{B^2} \right) = 0$$

A constant fraction of electrons are assumed to have power-law energy distribution

$$n(R, \pm z_1) = n_0 \exp\left[-\frac{(R - R_p)^2}{2\Delta^2} \right]$$

- $z_1 = \Delta = 5\, r_g$: fixed
- R_p: varied

Dependence on BH spin parameter

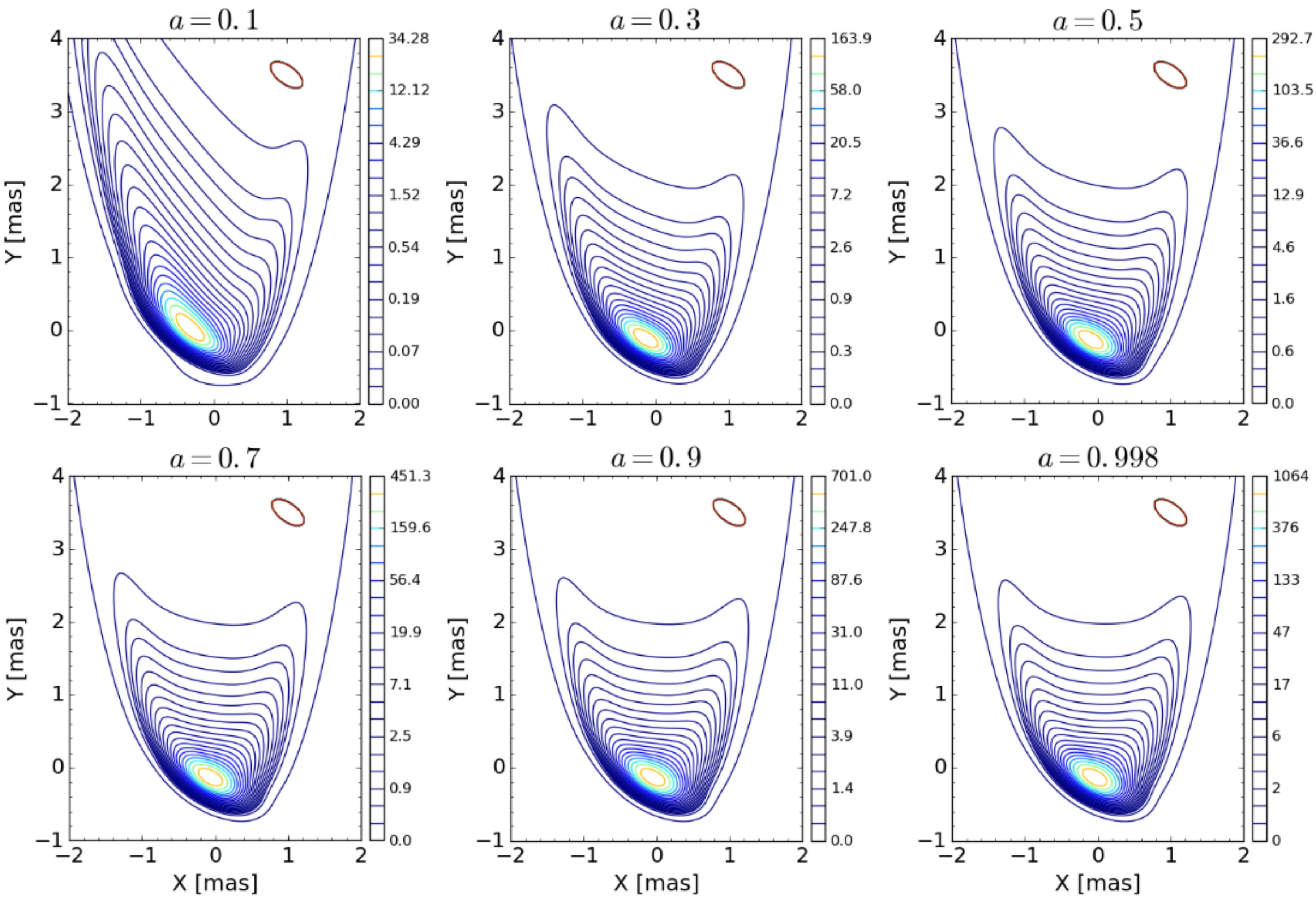

High BH spin parameter → Symmetric image

Turbulence cascade

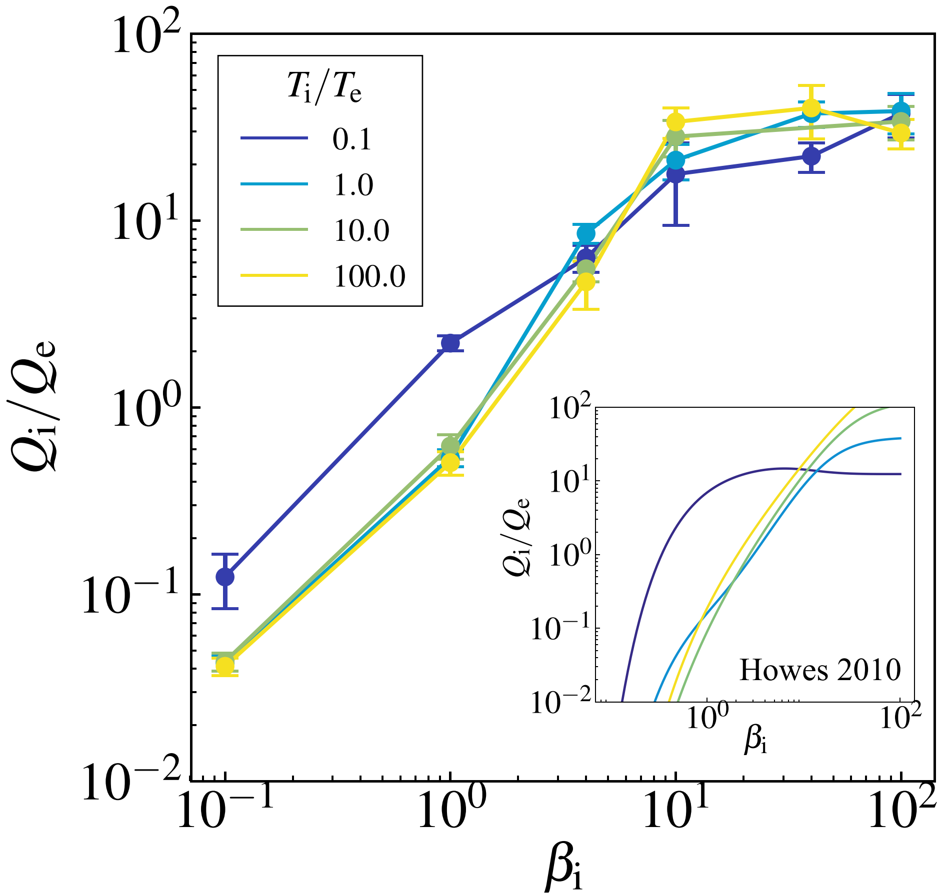

- Alfven turbulent cascade
- MHD inertial range
  -> ion Larmor scale
  (conversion to ion heating)
  -> kinetic Alfven waves
  (ultimately heating electrons)
- For low beta, ion thermal speed << Alfven speed, so that ions cannot interact with Alfvenic perturbations

Kawazura, Barnes & Schekochihin 2018

GRMHD code comparison

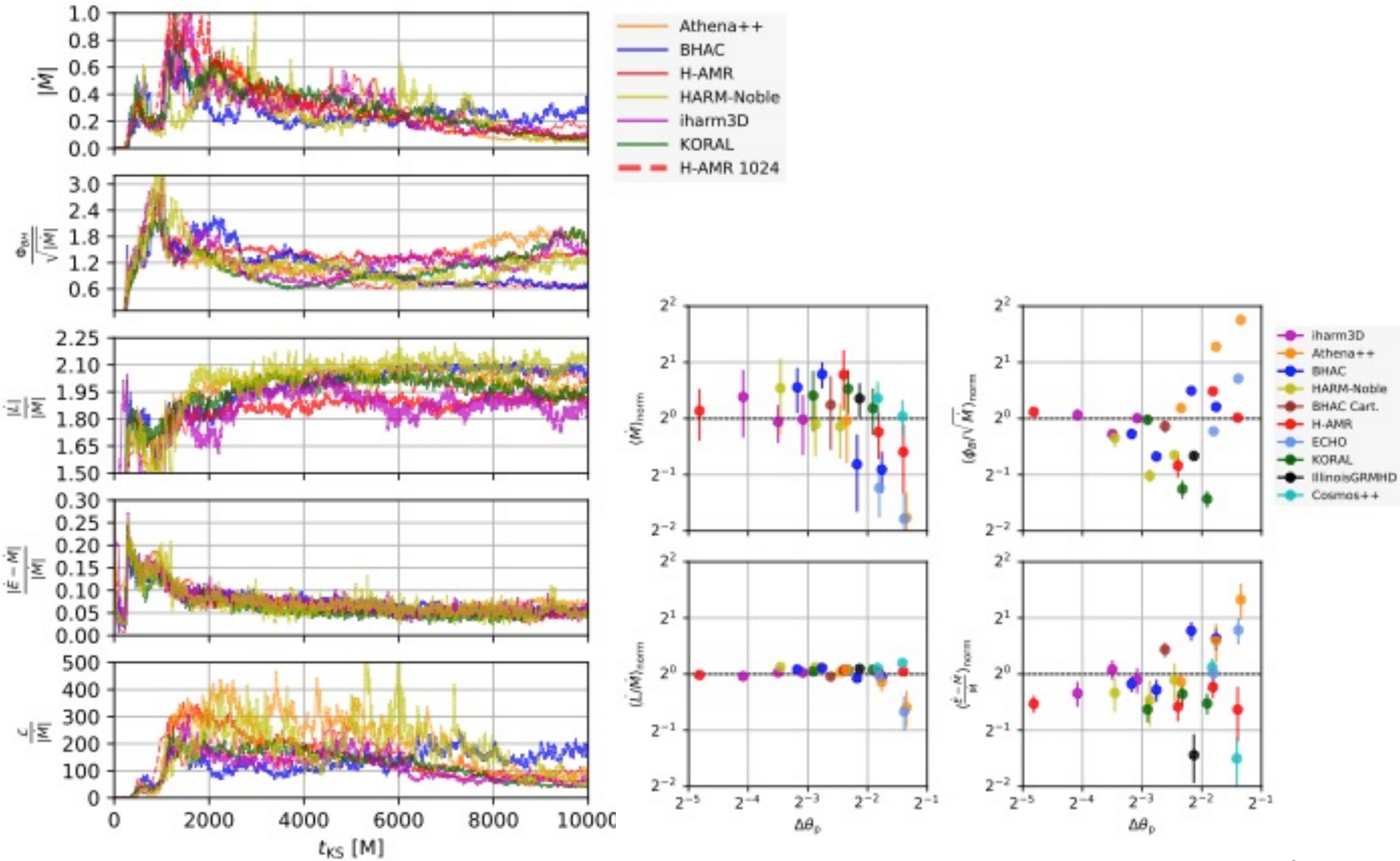

Porth+2019

Polarization

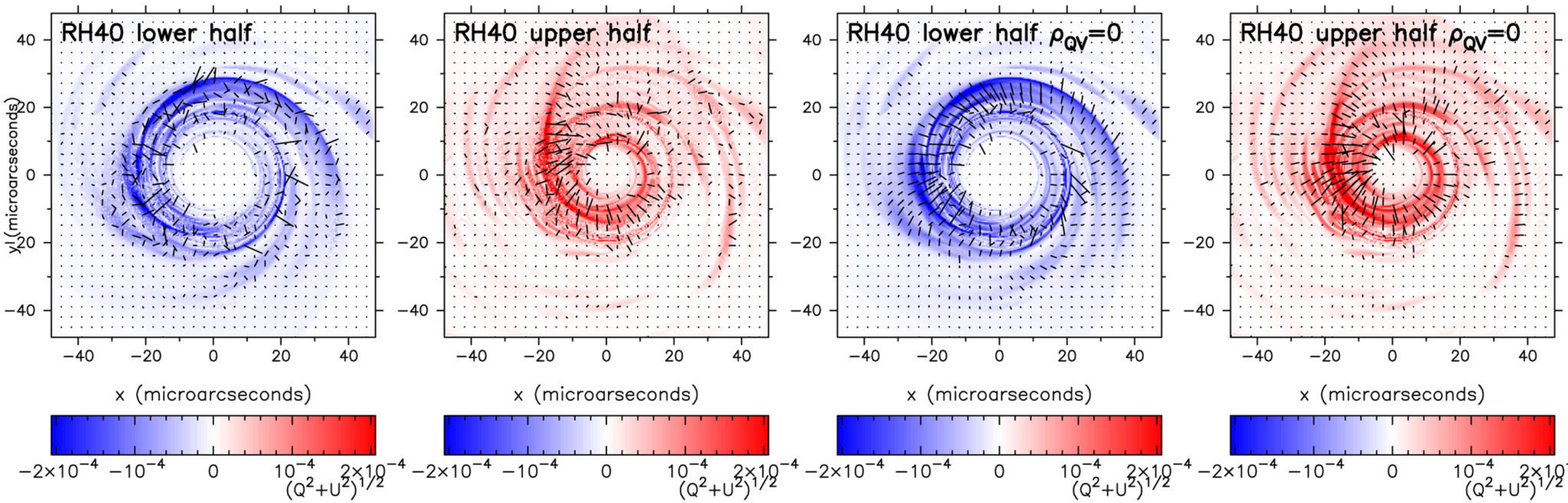

Figure 5. First and second panels: polarized emission $\sqrt{Q^2 + U^2}$ for each pixel originating from below (blue) and above (red) the mid-plane together with polarization ticks for model RH40. Third and fourth panels: same as first and second panels but with Faraday effects switched off. The model without Faraday effects shows coherent polarization signals from both counter and forward jets.

counter jet and forward jet. In Fig. 5, the counter-jet polarization (first panel) is evidently significantly scrambled compared to the coherent signal from the forward jet (second panel). The total LP degree from the counter jet is 1 per cent. This is smaller than the total polarization degree of the forward jet which is 3.1 per cent.

Moscibrodzka, Dexter, Davelaar & Falke 2017

Black Hole Shadow

Non-spinning Black Hole

Maximumly Rotating Black Hole

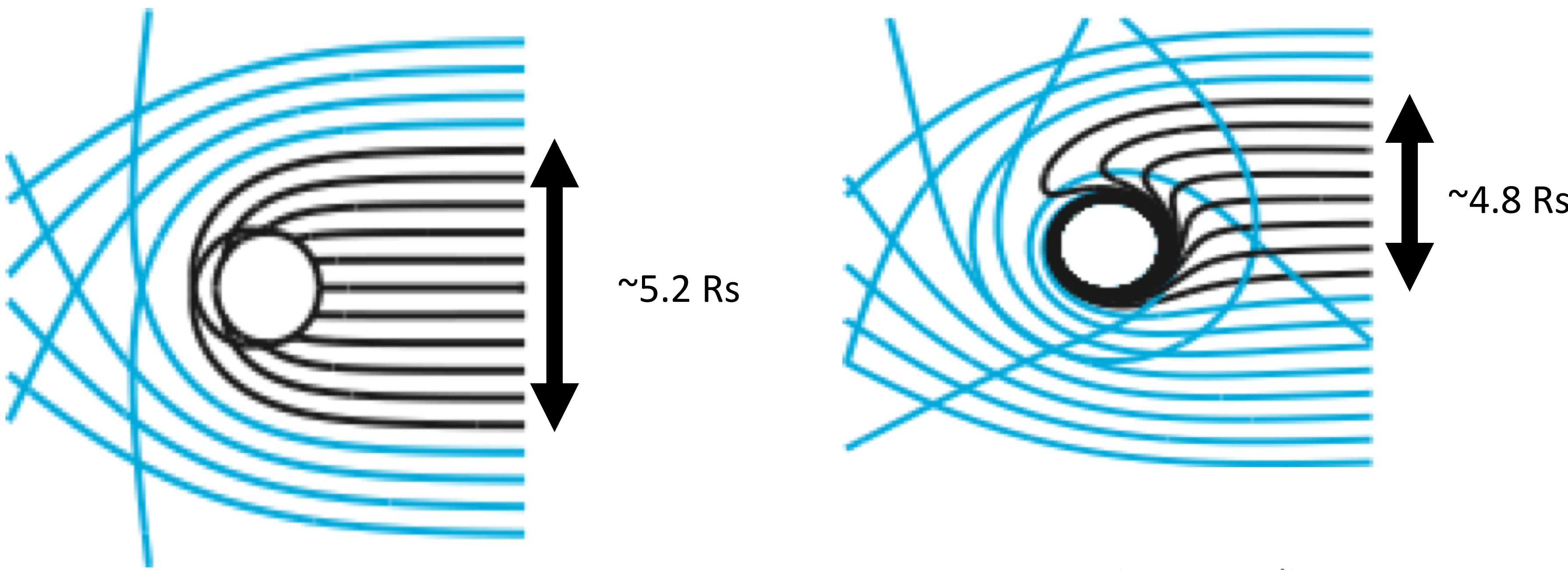

Figure credit: H.-Y. Pu